1138

NEANDC (E) 211 «L»
INDC (FR) 41/L

PROGRESS REPORT OF RECENT WORKS ON ACTINIDE NUCLEAR DATA AT BRUYERES-LE-CHATEL

Service de Physique Neutronique et Nucléaire
Centre d'Etudes de Bruyères-le-Châtel
B.P. n^o 561
92542 MONTROUGE CEDEX, France

- MARCH 1981 -

COMMISSARIAT A L'ENERGIE ATOMIQUE
FRANCE

NEANDC (E) 211 «L»
INDC (FR) 41/L

PROGRESS REPORT OF RECENT WORKS ON ACTINIDE NUCLEAR DATA AT BRUYERES-LE-CHATEL

Service de Physique Neutronique et Nucléaire
Centre d'Etudes de Bruyères-le-Châtel
B.P. n^o 561
92542 MONTROUGE CEDEX, France

- MARCH 1981 -

COMMISSARIAT A L'ENERGIE ATOMIQUE
FRANCE

CEA - NEANDC (E) 211 "L" - INDC (FR) 41/L

COMPTE RENDU DE TRAVAUX RECENTS SUR LES DONNEES NUCLEAIRES DES ACTINIDES REALISES A BRUYERES-LE-CHATEL

Sommaire.- Ce rapport rassemble un certain nombre de travaux réalisés à Bruyères-le-Châtel sur la détermination de données nucléaires relatives aux Actinides. Un aperçu préliminaire de ces travaux a déjà été donné au 3ème Meeting du projet de recherche coordonnée AIEA-NDS sur l'Intercomparaison des Evaluations des Données Nucléaires Neutroniques des Actinides, qui s'est tenu à Vienne les 12 et 13 juin 1980. On trouvera dans ce rapport des résultats à la fois expérimentaux et théoriques aussi bien que d'évaluation. En ce qui concerne plus spécialement les évaluations de sections efficaces, certains de ces travaux ont été initiés dans le cadre d'un Accord de Recherche pour la période du 1er avril 1979 au 31 mars 1980.

1981 90 p.

Commissariat à l'Energie Atomique - France

CEA - NEANDC (E) 211 "L" - INDC (FR) 41/L

PROGRESS REPORT OF RECENT WORKS ON ACTINIDE NUCLEAR DATA AT BRUYERES-le-CHATEL

Summary.- This report gathers a number of works dealing with the determination of actinide nuclear data which have been recently performed at Bruyères-le-Châtel. A preliminary outline of these works has already been reported on at the Third Meeting of the IAEA-NDS Coordinated Research Project on the Intercomparison of Evaluations of Actinide Neutron Nuclear Data which took place in Vienna, 12-13 june 1980. Experimental, theoretical as well as evaluation results will be found in this report. Concerning more specifically the cross sections evaluations, some of these works have been started in the framework of an IAEA-BRC Research Agreement for the period going from april 1st 1979 to march 31st 1980.

1981 90 p.

Commissariat à l'Energie Atomique - France

CONTENTS

INTRODUCTION AND SUMMARY

J. SALVY

This report gathers a number of works dealing with the determination of actinide nuclear data which have been recently performed at Bruyères-le-Châtel (BRC). A brief outline of these works has already been reported on [1],[2] by J. Salvy at the Third Meeting of the IAEA-NDS Coordinated Research Project (CRP) on the Intercomparison of Evaluations of Actinide Neutron Nuclear Data which took place in Vienna, 12-13 June 1980. Some of these works concerning more specifically the nuclear data evaluation have been undertaken in the framework of the IAEA-BRC Research Agreement 2072/CF for the period going from April 1st 1979 to March 31st 1980.

In chapters 1 to 4 the present status concerning measurements of various actinide data performed at BRC is given, namely :

- the $\bar{\nu}_p$ fission data and related quantities ($\bar{E}_\gamma$, $P(\nu)$,..), measured for a number of actinide isotopes, and their use as a basis for a semi-empirical evaluation in the case of fission induced by neutrons up to 15 MeV incident energy ;

- absolute fission cross section data, and their use to normalize other results ;

- (n,2n) and (n,3n) cross sections in the actinide region, with emphasis on the recent adaptation to fissile nuclei of the large Gd-loaded liquid scintillator method ;

- neutron elastic and inelastic scattering cross sections, including their theoretical interpretation by use of nuclear models and their usefulness for evaluating nuclear deformations.

Concerning the four topics above, the measurements which are being done or planned for the near future are mentionned.

In chaper 5 values of the width $\Gamma_{\gamma f}$ are deduced from recent experimental data related to the $(n,\gamma f)$ process in slow neutron induced resonances.

Results of recent ^{231}Pa fission cross section measurements performed at the Oak Ridge Electron linear Accelerator are given in chapter 6 along with some preliminary interpretation of the intermediate structure behaviour which is characteristic of the interaction of low energy neutrons with such a light actinide.

Chapter 7 is devoted to the description of the data retrieval system SYNOPSIS which has been worked out at BRC for storing and retrieving, in a form convenient for evaluation purposes, sets of data from several available files.

In chapters 8 to 11 results are given concerning the use of optical and statistical models for evaluating neutron nuclear data particularly in the actinide region. Some interpretation problems encountered at low energy are illustrated in chapter 8 concerning the interactions of 0.7 MeV energy neutrons with several fissile targets.

In chapter 9 a new evaluation procedure, the so called "fictitious even-even nucleus method", is presented in order to drastically simplify the use of the coupled channel optical model for evaluating neutron cross sections of odd-mass actinides. Such a method, which is less time consuming than "realistic" calculations, has been applied to the case of ^{241}Pu as described in chapter 10. Following a request [3] for comparing optical model calculations with spherical or deformed potentials, it is demonstrated by Ch. Lagrange in chapter 11 that inclusion of nuclear deformations is necessary for predicting actinide cross sections with enough confidence. Several examples are given which point out that noticeably better results are obtained with deformed optical potentials, particularly for obtaining correct mass and energy dependences of the compound nucleus formation cross sections. In cases where such "realistic" calculations could be considered as prohibitively time consuming, it is recommended to interpolate results, including generalized transmission coefficients needed for statistical model evaluations, obtained from well adapted deformed optical model calculations made for a few isotopes within the actinide region. Such a procedure is shown to be unexpectedly excellent when tested for ^{238}U.

Finally chapter 12 gives some actinide nuclear deformation characteristics as obtained at BRC from microscopic calculations based on the Hartree-Fock-Bogolyubov methods. The extension of such studies into the whole actinide region is to be recommended because of the following three points :

. important and encouraging progress have been achieved in the last years in the application of microscopic methods to predict bulk properties of heavy and deformed nuclei ;

. nuclear deformations, which vary smoothly through the actinide region, have been shown to significantly influence the behaviours of neutron cross sections ;

. much work is being devoted to a better understanding of the other optical and statistical parameters, and particularly concerning their variation from one actinide to another.

Other recent progress related to our knowledge of the actinide nuclear data will be found in the next BRC Annual Progress Report, to be published as an NEANDC-INDC report.

References

[1] Internal Report P2N-442/80 (May 1980).

[2] Report INDC(NDS)-119 (Oct. 1980).

[3] Report INDC(NDS)-104 (July 1979).

1/ PRESENT STATUS OF $\bar{\nu}_p$ DATA AT BRUYERES-LE-CHATEL

J. Fréhaut, A. Bertin, R. Bois

The measurements of $\bar{\nu}_p$ previously made at Bruyères-le-Châtel on the main isotopes of U and Pu [1,2] have been used as a basis for a semi-empirical evaluation of $\bar{\nu}_p$ for the fission induced by neutrons up to 15 MeV incident energy [3].

To check the validity of that evaluation for even-Z compound nuclei, a precise measurement of $\bar{\nu}_p$ for the fission of ^{237}Np induced by neutrons in the energy range from 1.5 up to 15 MeV has recently been performed [4]. A fission chamber associated with a large Gd-loaded liquid scintillator was used. The prompt signal from the liquid scintillator was used to determine the dependence of the prompt fission γ-ray average energy $\bar{E}_\gamma$ upon the incident neutron energy. The fission chamber contained a ^{252}Cf deposit, and the neutron detector efficiency was determined assuming a value of $\bar{\nu}_p = 3.732$ for the ^{252}Cf spontaneous fission.

The $\bar{\nu}_p$ data obtained are plotted in Fig. 1. The statistical accuracy is of the order of 0.6 %. A very good representation of the data is given by 4 lines as follows :

$E_n \leq 3.5$ MeV	:	$\bar{\nu}_p = 0.1415\ E_n + 2.5284$
3.5 MeV $\leq E_n \leq$ 6.1 MeV	:	$\bar{\nu}_p = 0.1714\ E_n + 2.4222$
6.1 MeV $\leq E_n \leq$ 12.2 MeV	:	$\bar{\nu}_p = 0.1544\ E_n + 2.5264$
12.2 MeV $\leq E_n$	:	$\bar{\nu}_p = 0.1200\ E_n + 2.9449$

However a single line of equation $\bar{\nu}_p = 0.1545\ E_n + 2.509$ also agrees within ± 1% with the experimental data.

The semi-empirical evaluation [3] : $\bar{\nu}_p = 0.1465\ E_n + 2.549$ is confirmed within ± 2% by the experimental results.

The prompt fission γ-ray energy $\bar{E}_\gamma$ is plotted as a function of the incident neutron energy in Fig. 2, along with the fission cross section. Below the (n,n'f) threshold, $\bar{E}_\gamma$ is a linear function of energy. Around the (n,n'f) threshold a plateau is appearing, and at higher energies, a linear function is observed again.

These results can be interpreted in terms of a competition between neutron and γ-ray emission in the desexcitation process of the fission fragments. From the experimental data for $\bar{\nu}_p$ and $\bar{E}_\gamma$ below the (n,n'f) threshold, one can deduce that :

$$\bar{E}_\gamma = 0.90\,\bar{\nu}_p + 4.40 \text{ (MeV)}$$

The value of 4.40 MeV corresponds to the statistical theory calculations. However, the neutrons are evaporated with a relatively small energy ($\sim$ 2 MeV) and do not reduce very much the spin of the fragments. At the end of the desexcitation process, the fragment angular momentum may be relatively high, and the γ-ray emission probability becomes large, even if the neutron emission is still energetically possible. The linear relationship between $\bar{E}_\gamma$ and $\bar{\nu}_p$ results from an increase of the average angular momentum of the fragments as a function of excitation energy.

In the (n,n'f) process, a fraction of the excitation energy of the compound nucleus is taken by the neutron evaporated prior to fission. The fission fragments will thus emit less neutrons and γ-ray energy, which explains the behaviour of $\bar{E}_\gamma$ between 5.5. and 8 MeV. However, the observed number of neutrons is not very affected, since the neutron evaporated before fission cannot be distinguished from the fission neutrons. The effect is more sensitive to the standard deviation σ of the fission neutron multiplicity distribution $P(\nu)$, as can be seen in Fig. 3 for ^{237}Np and ^{235}U : the behaviour of σ is comparable to the behaviour of E_γ .

The standard deviation of the $P(\nu)$ distributions obtained to date for various nuclei has been plotted as a function of $\bar{\nu}_p$ in Fig. 4. Only the data obtained below the (n,n'f) thresholds have been considered. On the average, σ is independent of the fissioning nucleus, and a satisfactory representation of the data is given by the linear relation : $\sigma = 0.12\,\bar{\nu}_p + 0.80$.

Finally, to complete this information on the $\bar{\nu}_p$ data let us mention the measurements made at Saclay in the resonance energy region for ^{239}Pu, ^{241}Pu and ^{235}U, and the study of the (n,γf) reaction [5,6].

A measurement of $\bar{\nu}_p$ in the threshold region for the neutron induced fission of ^{232}Th is presently in progress. The preliminary results show some structures in $\bar{\nu}_p$ as a function of incident neutron energy, which seem to be correlated to the relative contribution of the K = 1/2 and K = 3/2 channels to the fission cross section. In particular, a negative slope is observed below 1.7 MeV.

Future work includes the extension of the measurements on ^{232}Th up to 15 MeV incident neutron energy and a measurement on ^{243}Am in the energy range from threshold up to 15 MeV.

References of chapter 1

[1] M. Soleilhac, J. Fréhaut, J. Gauriau ; J. Nucl. Energ. 33 (1969) 257.

[2] J. Fréhaut, G. Mosinski, R. Bois, M. Soleilhac ; Rapport CEA-R-4626 (1974).

[3] R. Bois, J. Fréhaut ; Rapport CEA-R-4791 (1976).

[4] J. Fréhaut et al. ; Paper in preparation.

[5] J. Fréhaut and D. Shackleton ; Proc. Symp. on Physics and Chemistry of fission, Rochester (1973) Vol.2, p. 201.

[6] G. Simon and J. Fréhaut ; Proc. of the National Soviet Conference on Neutron Physics, Kiev (1975) Vol.5, p. 337.

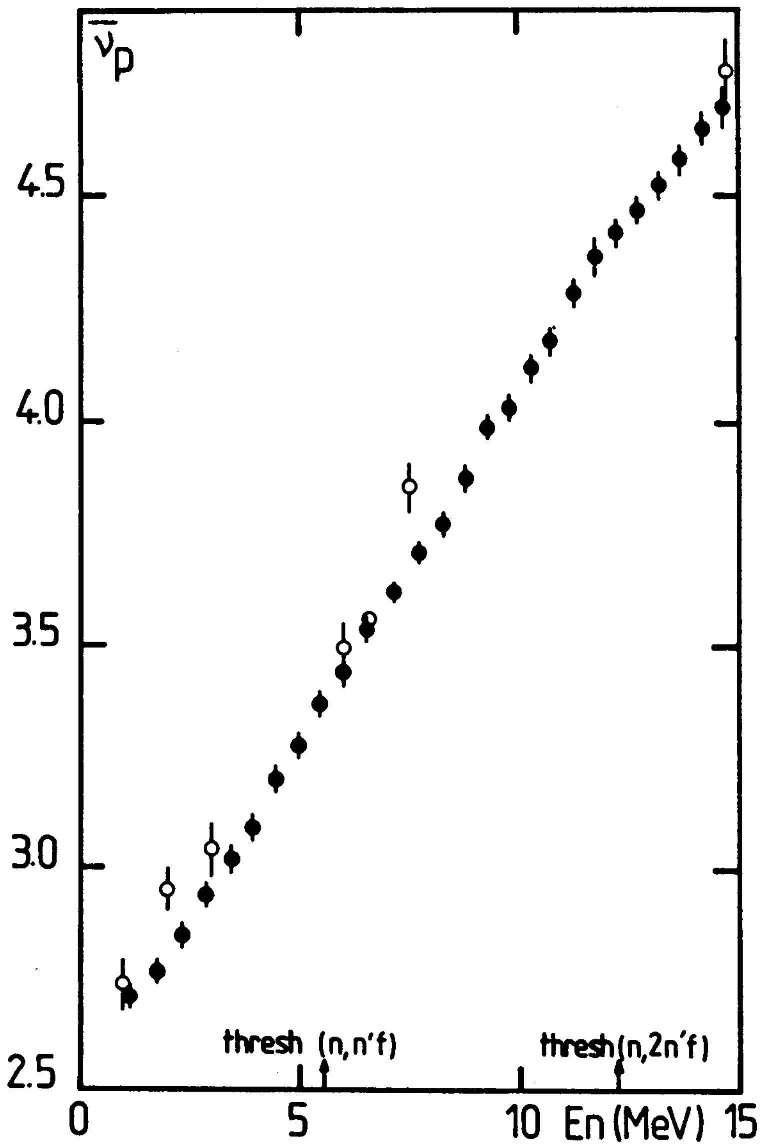

Fig. 1

Variation of $\bar{\nu}_p$ for the fission of ^{237}Np induced by neutrons in the energy range from 1 to 15 MeV.

● : present measurement

O : L. Veeser, Phys. Rev. C17 (1978) 385.

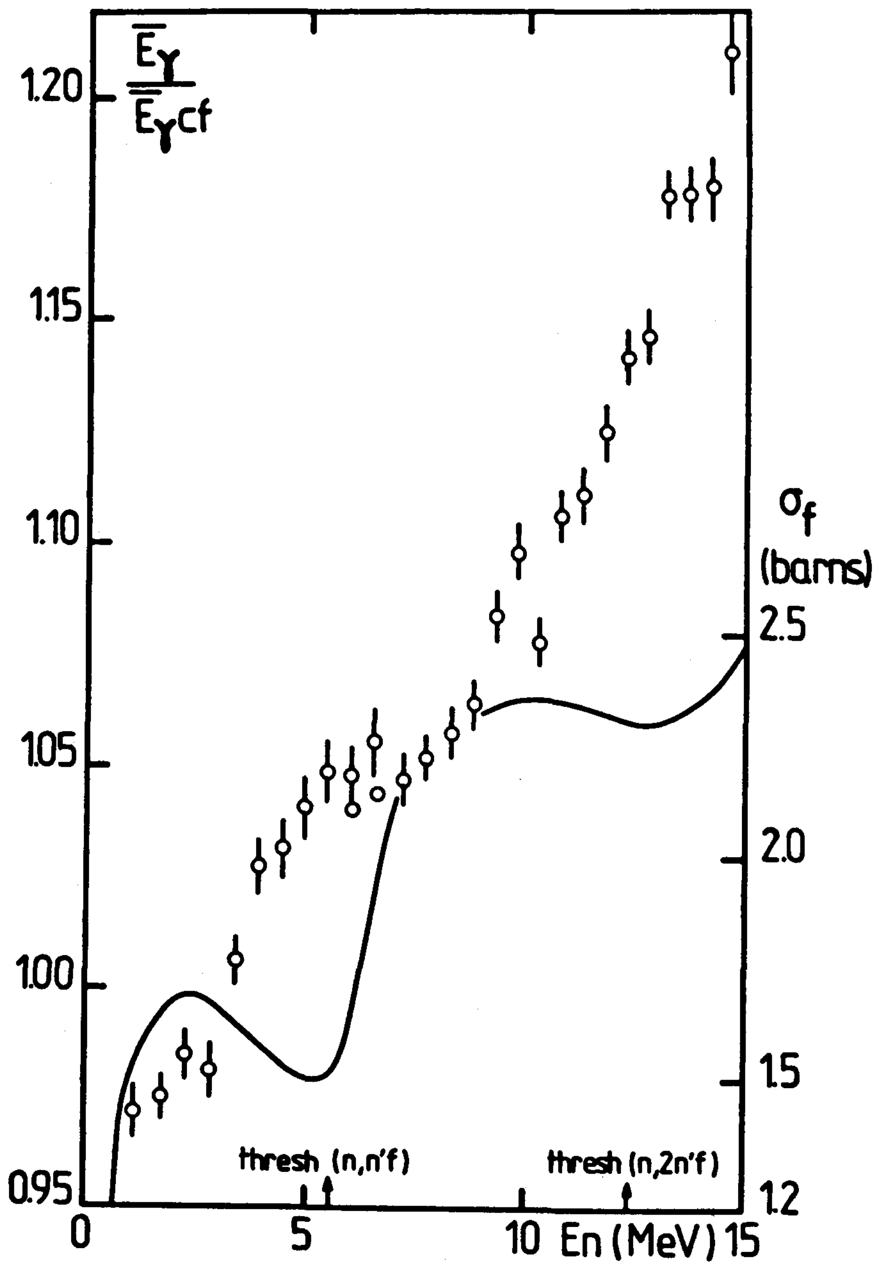

Fig. 2

Variation of the prompt fission gamma ray energy E_γ and of the fission cross section for the fission of ^{237}Np induced by neutrons in the energy range from 1 to 15 MeV. The $\overline{E}_\gamma$ values are normalized to the prompt γ-ray energy $\overline{E}_{\gamma cf}$ for the spontaneous fission of ^{252}Cf.

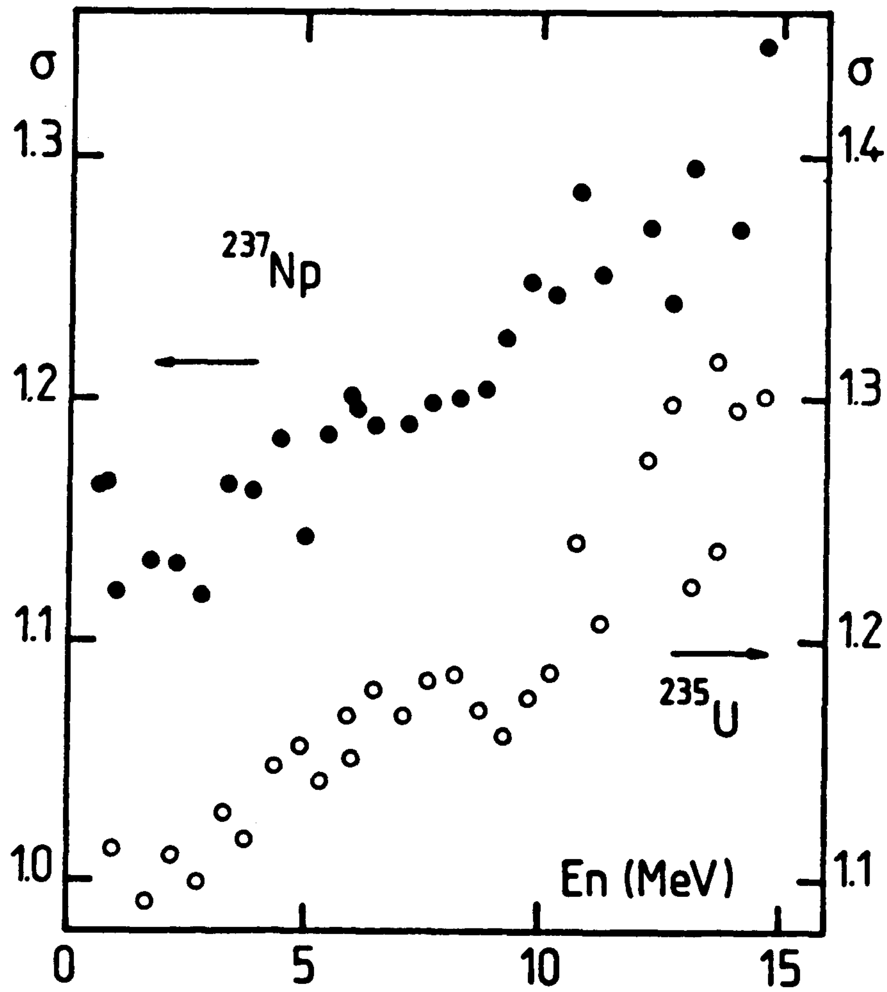

Fig. 3

Standard deviation of the fission neutron multiplicity distribution for the fission of ^{235}U and ^{237}Np induced by neutrons in the energy range from 1 to 15 MeV.

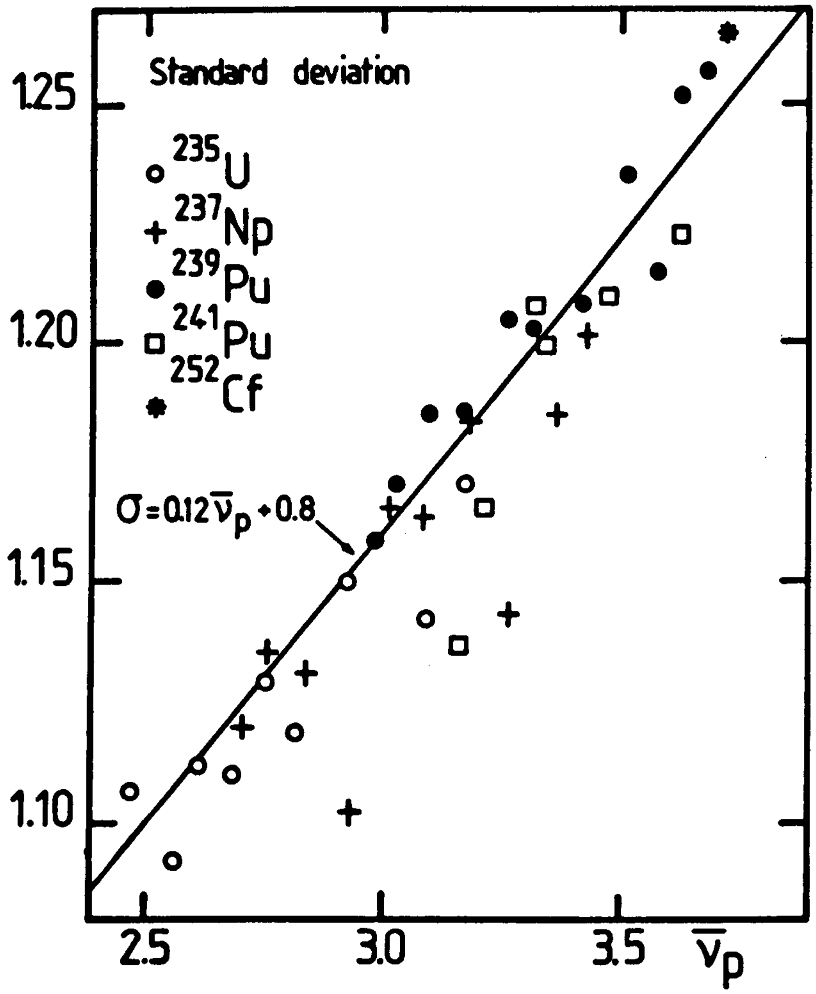

Fig. 4

Standard deviation of the P(ν) distributions as a function of $\bar{\nu}_p$.

2/ ABSOLUTE FISSION CROSS SECTIONS

M. Cancé, G. Grenier, D. Gimat and D. Parisot

2-1- Absolute neutron fission cross section of ^{235}U at 2.5 and 4.45 MeV

Recent measurements of ^{235}U fission cross sections still exhibit important differences (up to 8%) in the energy range of 2 to 6 MeV. So new absolute measurements are needed to resolve these discrepancies.

Two measurements have been made :

a) The first at 2.5 MeV in order to check our experimental method. Most of the data are found to be in agreement at this energy.

b) The second measurement was made at 4.45 MeV.

Detector system

A new detector system has been developed. Similar to Burton et al [1] we made a direct measurement of the ratio of fission to neutron-proton scattering cross sections with back-to-back deposits of ^{235}U and polyethylene. However, in our case, an ionization chamber replaces the solid state detector as fission fragments detector, in order to minimize the scattered neutrons.

This "hybrid detector" is shown in the figure 1. The radiator of polyethylene was 10μ thick. The first solid state detector of the proton recoil telescope was a ΔE type detector with a thickness of 50μ at 2.5 MeV and 150μ at 4.45 MeV (for this last case it was a special detector with an epoxy without hydrogen).

The second detector was 100μ thick. The ionization chamber was filled with a mixture of 90% Argon and 10% Methane at a pressure of $\simeq$ 0.6 atm.

^{235}U deposit

The uranium sample was an $\simeq$ 90μg/cm^2 thick uranium oxyde deposited on a 0.3 mm thick tantalum backing by "sputtering". The isotopic composition of uranium used is given in the table I.

The number of ^{235}U atoms was determined from low-geometry alpha counting using half-lives of uranium isotopes recommended by Vaninbroukx [2].

Radiator

The number of Hydrogen atoms in polyethylene radiator has been dedermined by Huffman Laboratory (Colorado).

Neutron source

A beam of pulsed neutrons with a pulse width of $\sim$ 1ns from the 4 MeV Van-de-Graaff accelerator was used for the measurements.

The 2.5 MeV neutrons were produced by the $T(p,n)^3He$ reaction using a (Ti-T) solid target. The 4.45 MeV neutrons were produced by the $D(d,n)^3He$ reaction using a gas target.

Experimental procedure

The detector system and the directional long counter were placed respectively at 0° to the beam direction at about 10 cm and 2 m. Indeed, at 2.5 MeV two references were used : the recoil proton detector and the directional long counter.

The time-of-flight method was used with the fission detector to determine the background due to uncorrelated fission events. An accurate background correction was obtained using a biparametric acquisition of pulse height and time pulses.

A clear identification of recoil protons was also obtained using a biparametric acquisition of the pulse height of both the proton detectors. At each energy two additional measurements have been made : one measurement without radiator and another without tritium or deuterium.

Corrections and uncertainties

The magnitudes of corrections needed in different cases are summarized in Table II. The loss of fission concerns the fraction of fragments absorbed in the deposit which is calculated with a Monte Carlo technique. The same technique is used to determine the fissions due to neutrons scattered by materials close to the uranium deposit. The errors in the cross section caused by the uncertainties in those corrections and the other errors are given in Table III.

Results

Total cross sections obtained with associated uncertainties are shown in Table IV. Our values are compared with other recent data in Fig. 2. These are in a good agreement with the ENDF-BV evaluation.

References of chapter 2-1

D.M. Burton et al. ; N.S.E. 60 (1976) 369.

R. Vaninbroukx ; EUR 5194e CBNM Geel (1974).

J.B. Czirr and G.S. Sidhu ; N.S.E. 57 (1975) 18. ; N.S.E. 58 (1975) 371.

W.P. Poenitz; N.S.E. 64 (1977) 894.

K. Kari ; KFK 2673, Karlsruhe (1978).

A.D. Carlson and B.H. Patrick ; Compte rendu de la Conference Internationale sur la Physique Neutronique et les Données Nucléaires pour les Reacteurs et autres Applications, Harwell 25-29 Septembre 1978.

2-2- Absolute neutron fission cross section of ^{241}Am at 14.6 MeV

Around 14 MeV, the measurements are fairly old and exhibit large discrepancies up to 20% between different measurements. Therefore a new absolute measurement was needed at this energy.

Experimental conditions

The fission detector is a gas scintillator filled with Xenon at a pressure of $\sim$ 1 atm. Fission events were detected by coincidence pulses from two photomultipliers. The ^{231}Am deposit was electrosprayed on a vyns foil. The characteristics of ^{241}Am deposit and backing are given in Table V. The number of ^{241}Am atoms was determined from low-geometry alpha counting. The absolute measurement was carried out with the associated particle technique [1]. The experimental arrangement is shown in Fig. 3. The 14.6 MeV neutrons were produced by T(d,n)^{4}He reaction with a 550 keV Van de Graaff accelerator. The time-of-flight method was used with the fission detector to determine the background due to uncorrelated fission events. The coincidence between the fast pulses furnished the start signal for the time-to-amplitude converter and the gating for the summed pulse height signals. An accurate background correction was obtained using a biparametric acquisition of summed pulse height and time pulses.

Corrections and uncertainties

The magnitudes of corrections needed in different cases are given in Table VI. The loss of fission events was obtained experimentally using a ^{235}U deposit. The errors in the cross sections caused by the uncertainties in those corrections and the other errors are given in Table VII.

Results

The absolute value of σ_{nf} (^{241}Am) obtained at 14.6 ± 0.13 MeV is (2.63 ± 0.12) barns. Our value, compared with previous data in Fig. 4, is in a good agreement with the relative measurements of Behrens [2].

References of chapter 2-2

[1] M. Cancé and G. Grenier ; NSE 68 (1978) 197.

[2] J.W. Behrens and J.C. Browne ; UCID 17324 (1976).

[3] E.F. Fomushkin et al. ; Soviet Journal of Nuclear Physics Vol. 5 (1967) 689.

[4] R.H. Iyer et al. ; Proceedings of the Nuclear Physics and Solid State Physics Symposium, University of Roorkee, India, December 28-31 (1969).

TABLE I : ISOTOPIC COMPOSITIONS AND AREA DENSITY OF DEPOSIT

ISOTOPIC COMPOSITION (at %)					AREA DENSITY $\mu g/cm^2$
Sample	^{234}U	^{235}U	^{236}U	^{238}U	U_3O_8
^{235}U	1.6653	97.663	0.1491	0.5229	103.2

TABLE II : MAGNITUDE AND NATURE OF CORRECTIONS

EFFECT	Correction (%)	
	E_n = 2.5 (MeV)	E_n = 4.45 (MeV)
Fission detector		
Extrapolation to zero pulse height	0.9	1.2
Loss of fissions	0.7	0.7
Fissions due to other isotopes	2.3	2.4
Fission due to scattered n	4.7	3.4
Fission without T or D (target)	0.1	7.4
Telescope		
Events without radiator	9.3	12
Events without T or D	0.6	2.8
Neutron attenuation in deposit backing	1.5	1.3
Directional long counter		
Background without T or D	0.4	
Background without shadow bar	4	
Neutron attenuation		
in air	2.7	
in detector system	2.7	

TABLE III : UNCERTAINTIES

EFFECT	Uncertainty (%) 2.5 (MeV)	4.45 (MeV)
Fission detector		
Extrapolation to zero pulse height	0.1	0.1
Loss of fissions	0.1	0.1
Fissions due to others isotopes	0.2	0.2
Fissions due to scattered n	0.5	0.3
Fission without T or D in target	–	0.7
Atoms number of ^{235}U	0.5	0.5
Statistical	0.7	1.1
Geometrical factors	0.5	0.4
Telescope		
Events without radiator	0.9	1.2
Events without T or D	0.1	0.3
Neutron attenuation in deposit backing	0.1	0.1
$\sigma(n, p)$	0.75	0.75
Atoms number of H	0.2	0.2
Efficiency	0.3	0.3
Statistical	0.3	0.5
Directional long counter		
Background without T or D	-	
Background with shadow bar	0.4	
Neutron attenuation		
in air	0.3	
in detector system	0.3	
Efficiency	2.5	

TABLE IV : TOTAL UNCERTAINTIES AND RESULTS

Neutron energy	2.5 ± 0.04 (MeV)		4.45 ± 0.1 (MeV)
Neutron detector	Telescope	Long counter	Telescope
Total Uncertainty	1.7 *	2.8 *	2.2 *
σ_{nf} (^{235}U)	1.28 ± 0.02	1.23 ± 0.03	1.13 ± 0.03

* The errors are added quadratically

TABLE V

CHARACTERISTICS OF 241 Am DEPOSIT AND BACKING	
DEPOSIT	
- CHEMISTRY FORM...	ACETATE
- METHOD OF DE. POSITION	ELECTROSPRAYING
- THICKNESS.........	12.32 $\mu g/cm^2$
- DIAMETER.........	60 mm
- ATOM DENSITY..... (T = 432 ±4 years)	$0.170247 . 10^{17}$
BACKING	
- PLASTIC (VYNS)....	20 $\mu g/cm^2$
- Al	20 $\mu g/cm^2$

TABLE VI

RANGE OF CORRECTIONS	
EFFECT	CORRECTIONS %
LOSS OF FISSION	19.27
BACKGROUND T.O.F.	10.01
NEUTRON ATTENUATION :	
- target backing	0.61
- plastic surrounding the detector	0.23
- front face of gas scintillator	2.02

TABLE VII

RANGE OF UNCERTAINTIES	
EFFECT	% (at 1σ)
LOSS OF FISSION............	2.71
STATISTIC..................	2.6
ATOMS NUMBER.............	2.5
NEUTRON ATTENUATION	
- target backing	0.61
- plastic	0.02
- front face of gas scintillator	0.2
TOTAL.....................	4.52

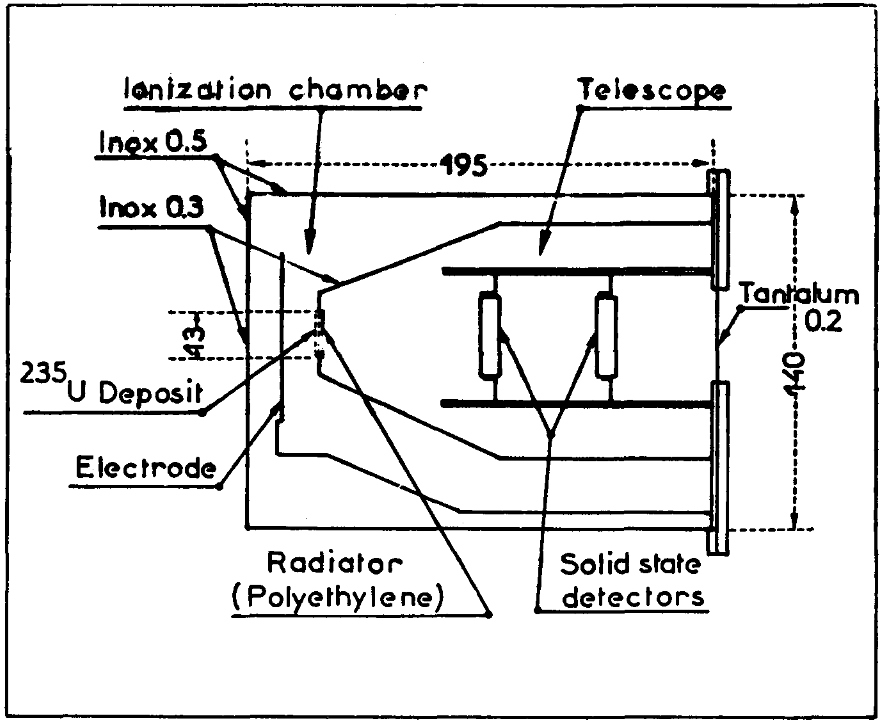

Fig. 1

Hybrid detector

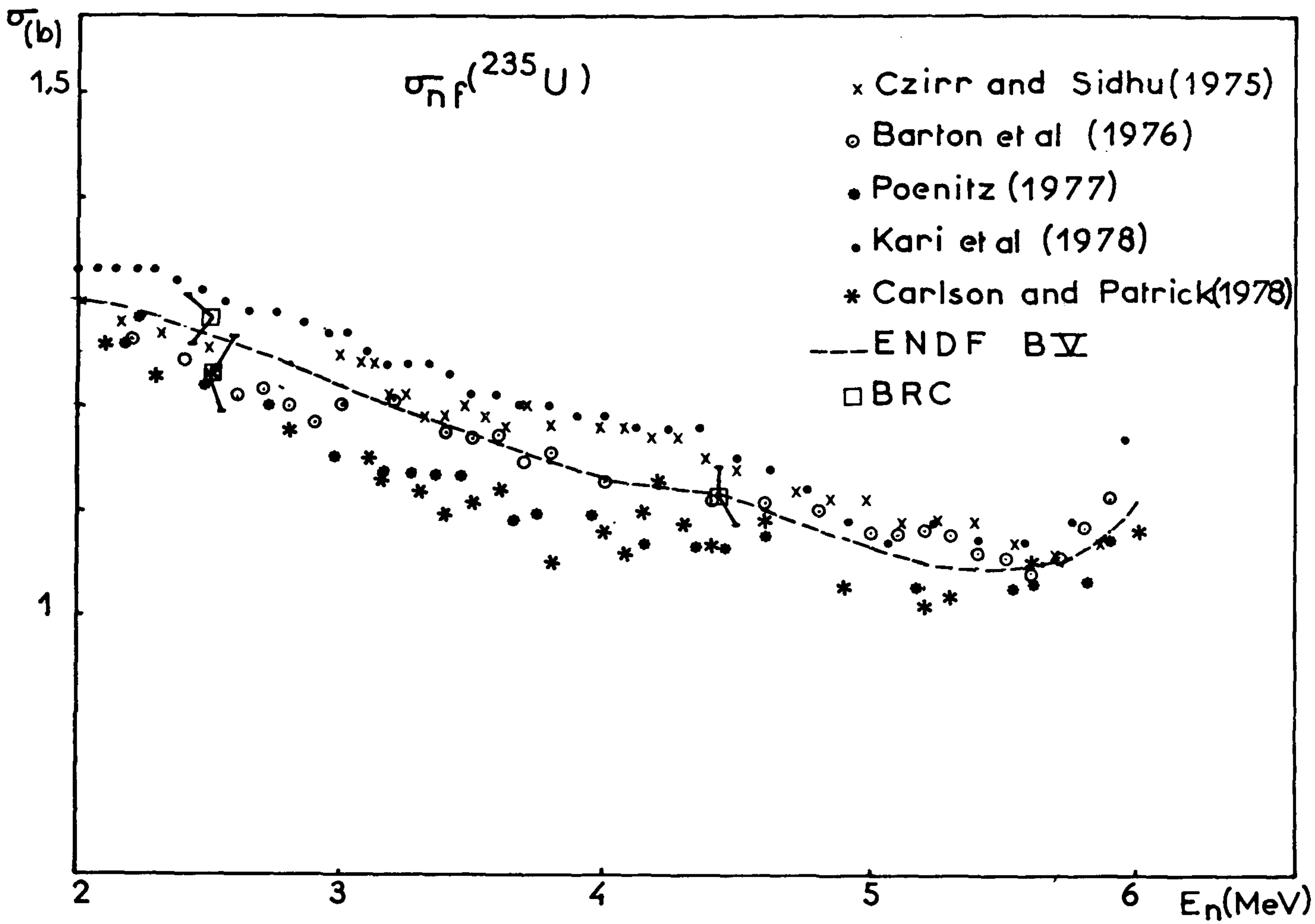

Fig. 2

Fission cross section of ^{235}U between 2 and 6 MeV

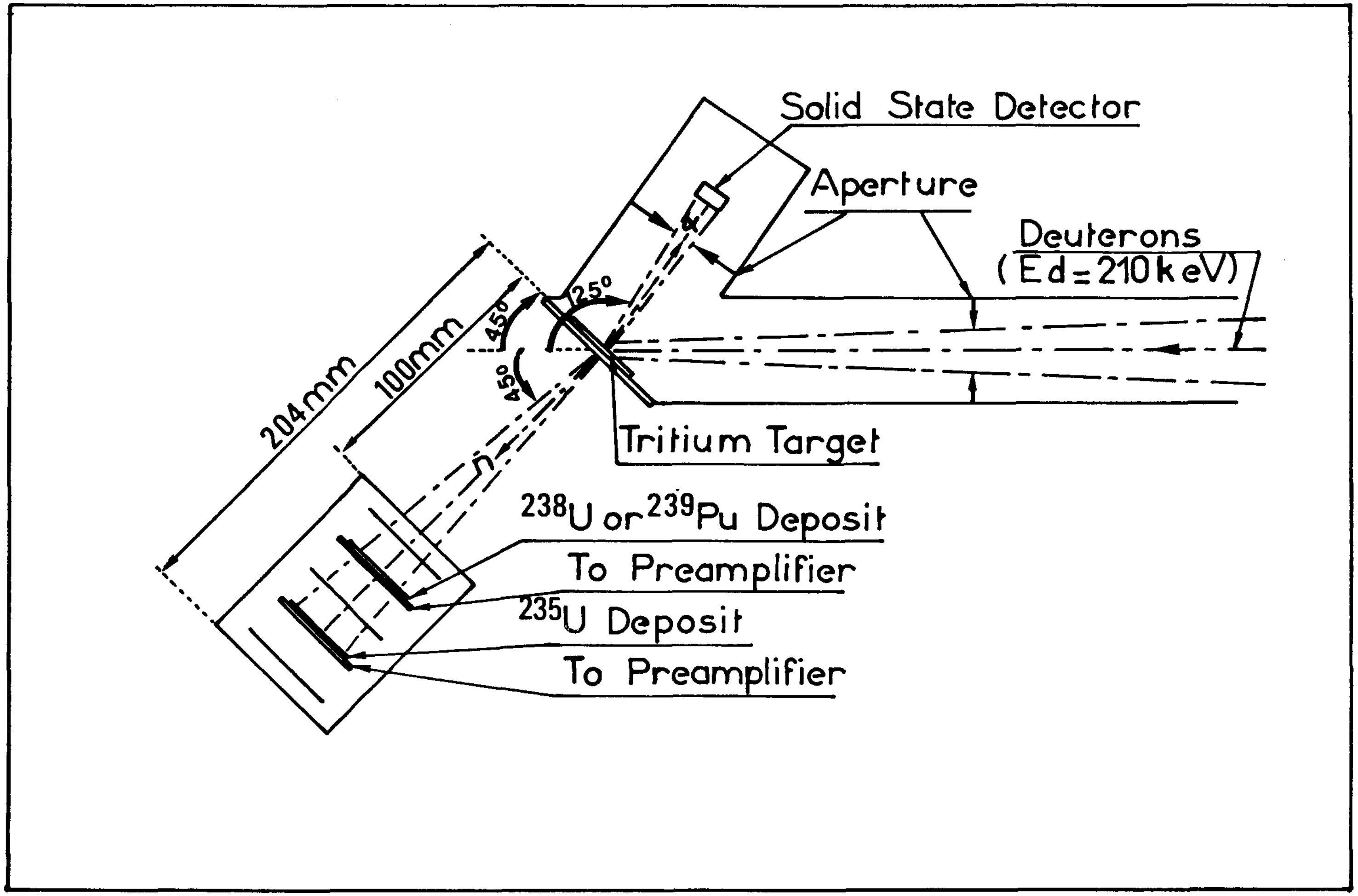

Fig. 3

Experimental arrangement

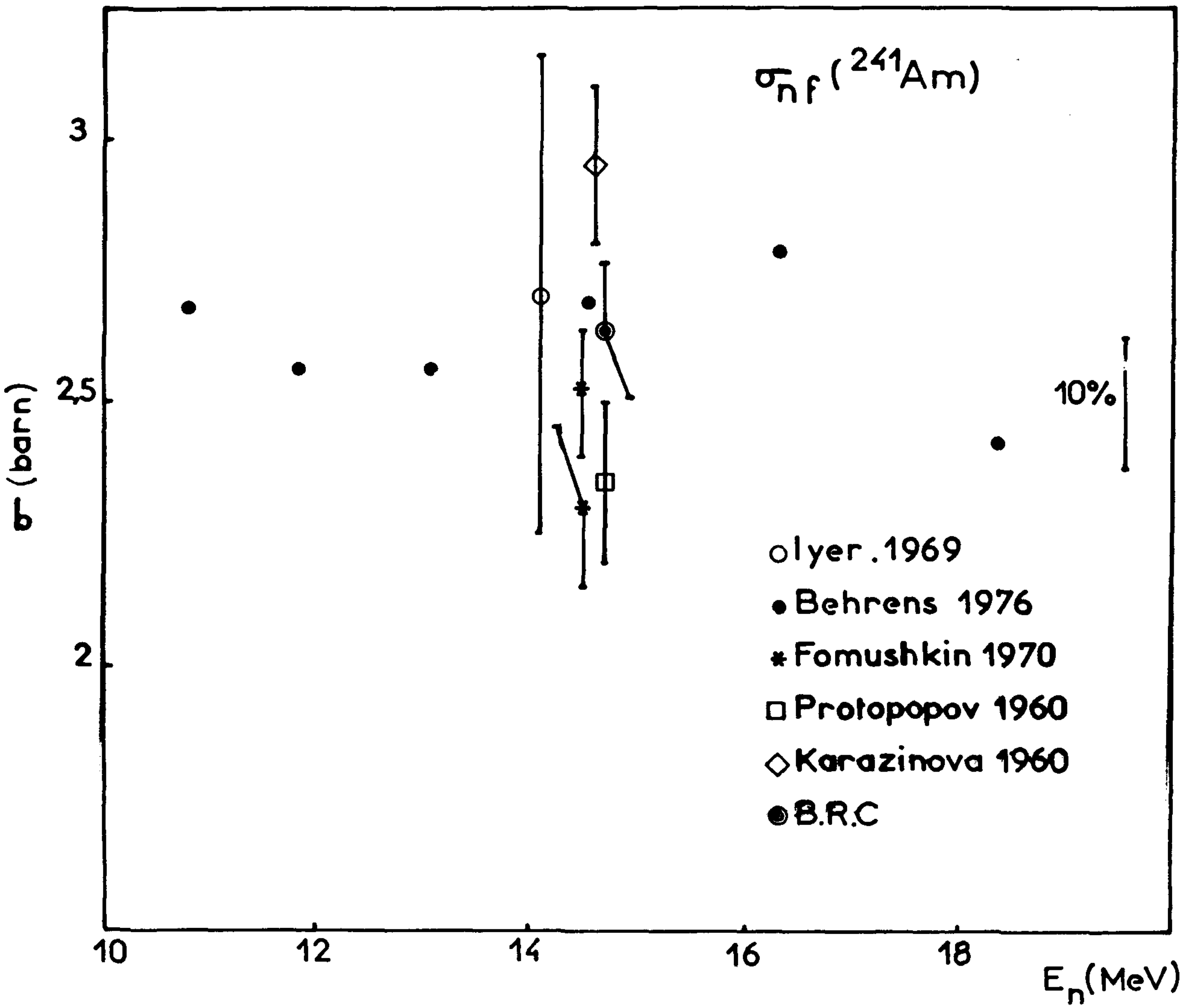

Fig. 4

Fission cross section of ^{241}Am between 10 and 18 MeV

3/ STATUS OF (n,xn) CROSS SECTION DATA AT BRUYERES-LE-CHÂTEL IN THE ACTINIDE REGION

J. Fréhaut

In late years, the large Gd-loaded liquid scintillator method has been developed at Bruyères-le-Châtel for (n,xn) cross section measurements in the energy range below 15 MeV [1].

The method relies on the measurement of the neutron multiplicity of the individual induced events.

In the particular case of fissionable materials, fissions can also be induced during the incident neutron pulses, yielding a number of neutrons from 1 to about 10, which cannot be experimentally distinguished from those of (n,2n) or (n,3n) reactions.

However, events with more than 3 neutrons can only result from fission in the incident neutron energy range below 15 MeV considered here. The total number of fissions can thus be calculated from the distributions of events with more than 3 neutrons, by using the fission neutron multiplicity distributions previously measured [2]. The number of fissions giving 2 or 3 neutrons can then be determined and subtracted from the observed rate, to give the true number of (n,2n) and (n,3n) events.

This method provides directly the ratio of the (n,2n) or (n,3n) cross section to the fission cross section.

To avoid an absolute measurement of the incident neutron flux, all the (n,xn) cross sections measured to date (about 50 nuclei) have been normalized to the ^{238}U fission cross section, by including a run with an uranium sample in every series of measurements [3]. Thus, the (n,2n) and (n,3n) cross sections for ^{238}U have been extensively measured. The resulting data are given in Table I.

The method has recently been adapted for measurements on fissile nuclei. In that case, the presence of fissions induced by the low energy neutrons contaminating the incident beam disturbs the fission neutron multiplicity distribution and increases the apparent fission cross section. This component could be evaluated by normalizing the cross section measured for a given nucleus at the same time to its fission cross section and to that of ^{238}U, and by assuming that the two values obtained should be statistically equal [4]. The (n,2n) cross section of ^{235}U has been measured in the energy range from threshold to 13 MeV. The data are given in Table II [4].

Measurements are planned in the near future on ^{232}Th and ^{239}Pu, and on ^{237}Np in 1981.

References of Chapter 3

[1] J. Fréhaut ; Nucl. Inst. Meth. 135 (1976) 511.

[2] M. Soleilhac, J. Fréhaut, and J. Gauriau ; J. Nucl. Energ. 23 (1969) 257.

[3] J. Fréhaut, A. Bertin, R. Bois, and J. Jary ; paper presented at the Symposium on Neutron Cross Sections from 10-50 MeV, Brookhaven, May 1980.

[4] J. Fréhaut, A. Bertin, R. Bois ; to be published in Nucl. Sc. Engin.

[5] M. G. Sowerby, B.H. Patrick, and D.S. Mather ; Report AERE-R-72/73 (1973), Harwell, UKAEA.

TABLE I

E_n (MeV)	σ(n,2n) mb	σ(n,3n) mb
6.89 ± 0.185	233 ± 39	
7.41 ± 0.165	604 ± 54	
7.67 ± 0.160	811 ± 62	
7.93 ± 0.150	879 ± 48	
8.18 ± 0.145	999 ± 41	
8.44 ± 0.135	1072 ± 52	
8.69 ± 0.130	1029 ± 60	
8.94 ± 0.125	1156 ± 42	
9.44 ± 0.115	1171 ± 46	
9.93 ± 0.110	1232 ± 44	
10.42 ± 0.100	1258 ± 48	
10.91 ± 0.095	1260 ± 44	
11.40 ± 0.090	1300 ± 52	
11.88 ± 0.085	1324 ± 48	30 ± 09
12.36 ± 0.085	1313 ± 66	69 ± 13
12.85 ± 0.080	1272 ± 56	172 ± 24
13.33 ± 0.075	1134 ± 58	295 ± 32
13.80 ± 0.075	925 ± 54	389 ± 36
14.28 ± 0.070	790 ± 66	500 ± 46
14.76 ± 0.065	642 ± 64	568 ± 50

Experimental (n,2n) and (n,3n) cross sections for ^{238}U normalized to the ^{238}U fission cross section [5].

TABLE II

$E_n \pm \Delta E_n$ (MeV)	$\sigma_{n,2n'}$ barn
5.73 ± 0.090	0.004 ± 0.024
5.98 ± 0.090	0.128 ± 0.023
6.49 ± 0.085	0.273 ± 0.030
7.01 ± 0.080	0.355 ± 0.032
7.52 ± 0.075	0.463 ± 0.034
8.03 ± 0.075	0.482 ± 0.038
8.54 ± 0.070	0.614 ± 0.052
9.04 ± 0.065	0.642 ± 0.043
9.55 ± 0.065	0.734 ± 0.048
10.06 ± 0.060	0.772 ± 0.055
10.56 ± 0.060	0.775 ± 0.055
11.07 ± 0.055	0.857 ± 0.066
11.57 ± 0.055	0.870 ± 0.071
12.08 ± 0.055	0.857 ± 0.085
12.58 ± 0.050	0.863 ± 0.109
13.09 ± 0.050	0.717 ± 0.110

Experimental (n,2n) cross section for ^{235}U normalized to the ^{238}U fission cross section [5].

4/ NEUTRON SCATTERING DATA FOR ACTINIDE NUCLEI

G. Haouat, Y. Patin, J. Lachkar, J. Sigaud, J. Jary, Ch. Lagrange

An extensive experimental study of fast neutron scattering from actinide nuclei has been undertaken in order to fulfil cross sections needs and to provide a correct description of the neutron-nucleus interaction in this mass-region.

Differential cross sections have been measured for the elastic and inelastic scattering from the isotopes ^{232}Th, ^{233}U, ^{235}U, ^{238}U, ^{239}Pu and ^{242}Pu at various energies ranging between 0.6 and 3.4 MeV. The energies were chosen according to the respective importance of the compound-nucleus and direct-interaction mechanisms estimated for the elastic scattering cross sections and the inelastic scattering cross sections to the low-lying collective states.

The experimental conditions were fixed so as to obtain a good separation of the elastic and inelastic scattering neutron groups for the even-even actinides and ^{233}U for which the energy spacing of the ground and first excited states is around 40 keV. The energy resolution of the neutron time-of-flight spectrometer varied between 10 keV at 0.7 MeV incident energy and 28 keV at 3.4 MeV. Time-of-flight spectra for the ^{238}U sample are shown in figure 1 to illustrate the experimental resolution at 0.7 and 3.4 MeV.

Differential cross sections for neutron scattering from ^{232}Th and ^{238}U were measured at 0.7 - 1.5 - 2.5 and 3.4 MeV in the angular range from 20° to 160°. Cross sections were obtained for the elastic scattering and inelastic scattering to the first 2^+ and 4^+ states of these isotopes. Figure 2 shows the data for ^{238}U.

Measurements on ^{233}U were performed at 0.7 and 1.5 MeV between 20° and 160°. Cross sections were obtained for the elastic scattering ($5/2^+$) and the inelastic scattering to the first $7/2^+$ (40 keV) and $9/2^+$ (92 keV) excited states.

For ^{235}U, data were taken at 0.7 and 3.4 MeV in the angular range 20°-160°. Because at both energies the experimental resolution is larger than the energy spacing of some levels of ^{235}U, cross sections were determined for the two groups of levels ($7/2^-$ g.s. - $1/2^+$, 75 eV - $3/2^+$, 13 keV) and ($9/2^-$, 46 keV - $5/2^+$, 52 keV) ; also cross sections were obtained at 3.4 MeV for the excited state $11/2^-$, 103 keV. However, both the 0.7 and 3.4 MeV time-of-flight spectra seem to indicate that the states of the rotational band built on the $1/2^+$ (75 eV) single particle level are very weakly excited.

Data were taken for ^{239}Pu at 0.7 and 3.4 MeV. The 3.4 MeV cross sections were obtained for three groups of levels : ($1/2^+$ g.s. - $3/2^+$, 8 keV),

($5/2^+$, 52 keV - $7/2^+$, 76 keV) and ($9/2^+$, 163 keV - $11/2^+$, 173 keV). But at 0.7 MeV, the experimental resolution permitted the separation of the contributions from the various levels and angular distributions were determined for the ground state, $1/2^+$, and the excited states $3/2^+$, $5/2^+$, $7/2^+$. The data appear in figure 3.

Differential cross sections for ^{242}Pu were measured at 0.6 - 1.0 - 1.5 - 2.0 and 2.5 MeV in the angular range from 15° to 160°. Extraction of the ^{242}Pu scattering yields was difficult because the time-of-flight spectra contain neutron peaks corresponding to the scattering from stainless steel and carbon of the container and from oxygen of the Pu O_2 sample. Figure 4 gives the 2.5 MeV data for the elastic scattering and the inelastic scattering to the first 2^+ state (44.5 keV).

The present data have been compared to the evaluations ENDF/BIV and ENDL/76 : large discrepancies appear mainly at high energies [1]. Figure 5 shows our 3.4 MeV elastic scattering cross sections for ^{232}Th, ^{235}U, ^{238}U and ^{239}Pu along with the angular distributions obtained from the ENDF/BIV (dotted lines) and ENDL 76 (dashed lines) files.

A theoretical analysis of the present data has been carried out for the nuclei ^{232}Th, ^{235}U, ^{238}U and ^{239}Pu. Both the direct-interaction (DI) and compound-nucleus (CN) processes were considered in the calculations. The coupled-channel optical model was used to estimate the DI cross sections and the Wolfenstein-Hauser-Feshbach formalism, with width-fluctuation corrections and generalized neutron penetrabilities from the optical model calculations, for computing the CN cross sections. Potential depths and deformation parameters thus deduced are given in table 1. The values of the optical potential depths are very similar ; the slight differences one can notice might be ascribed to an isospin dependence. Thus except for the potential deformations, these nuclei have the same behaviour with respect to neutron scattering. Concerning the potential deformations a comparison of the quadrupole deformation parameters (table 1) shows that the static deformation is rather larger for the even-odd nuclei than for the even-even ones. This difference must be emphasized in further evaluations for transactinides.

For ^{242}Pu the 2.5 MeV data are compared in fig. 4 to calculations performed with the deformed potential parameters previously given by Lagrange and Jary in their evaluation of ^{240}Pu and ^{242}Pu cross sections [2] ; these parameters are given in table 1. The agreement between measurements and calculations is fairly good (fig. 4) although a better fit to the angular distributions would yield more reliable values of the ^{242}Pu deformation parameters.

References of chapter 4

[1] G. Haouat, J. Sigaud, J. Lachkar, Ch. Lagrange, B. Duchemin, Y. Patin ; Report NEANDC(E) 180"L", INDC(FR) 13L (1977).

G. Haouat, J. Lachkar, Ch. Lagrange, Y. Patin, J. Sigaud, R.E. Shamu ; Report NEANDC(E) 196"L", INDC(FR) 29/L (1978).

[2] Ch. Lagrange, J. Jary ; Report NEANDC(E) 198"L", INDC(FR) 30/L (1978).

TABLE I

Geometric parameters / nucleus	V_R : REAL POTENTIAL	W_D : SURFACE IMAGINARY POTENTIAL	V_{SO} : SPIN-ORBIT POTENTIAL	QUADRUPOLE DEFORMATION (β_2)	HEXADECAPOLE DEFORMATION (β_4)
	$R_R^\circ = 1.26$ $a_R = 0.63$	$R_D^\circ = 1.26$ $a_D = 0.52$	$R_{SO}^\circ = 1.12$ $a_{SO} = 0.47$		
^{232}Th	$46.4(\pm 0.2) - 0.3\,E$	$3.6(\pm 0.2) + 0.4\,E$	6.2 ± 0.3	0.190 ± 0.010	0.071 ± 0.007
^{235}U	$46.4(\pm 0.2) - 0.3\,E$	$3.3(\pm 0.2) + 0.4\,E$	6.2 ± 0.3	0.220 ± 0.011	0.080 ± 0.008
^{238}U	$46.2(\pm 0.2) - 0.3\,E$	$3.6(\pm 0.2) + 0.4\,E$	6.2 ± 0.3	0.198 ± 0.010	0.057 ± 0.006
^{239}Pu	$46.2(\pm 0.2) - 0.3\,E$	$3.6(\pm 0.2) + 0.4\,E$	6.2 ± 0.3	0.220 ± 0.011	0.070 ± 0.007
^{242}Pu	$46.0(\pm 0.2) - 0.3\,E$	$3.5(\pm 0.2) + 0.4\,E$	6.2 ± 0.3	0.204 ± 0.010	0.051 ± 0.005

Deformed potential parameters used in this study. Radii and diffusivenesses are given in fm. Potential depths and incident neutron energy E are given in MeV. Also given are the quadrupole (β_2) and hexadecapole (β_4) deformations of the optical potential.

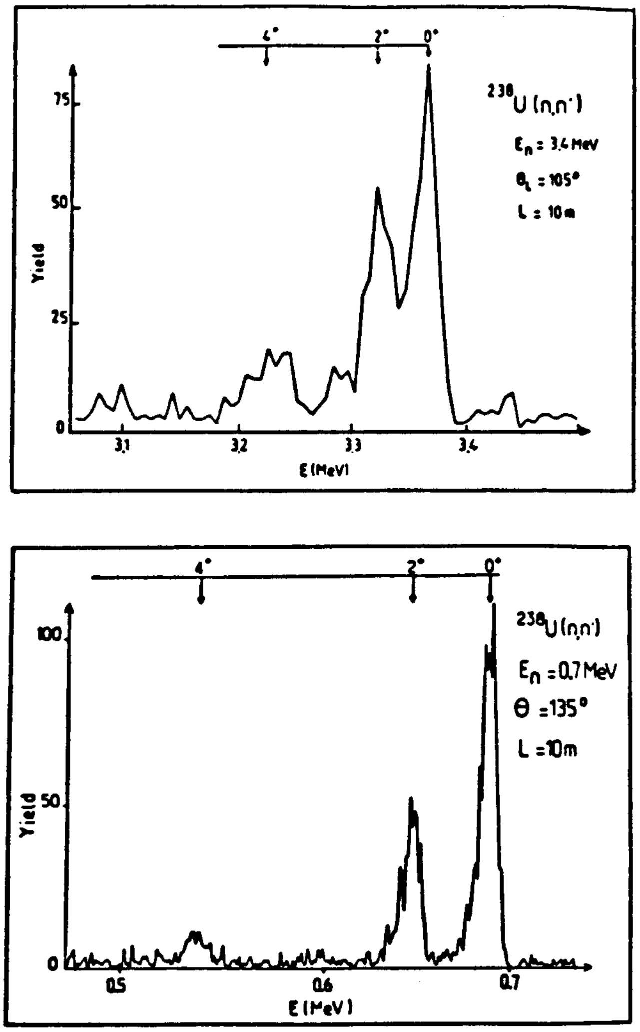

Fig. 1

Time-of-flight spectra of 3.4 MeV (above) and 0.7 MeV (below) neutrons scattered from ^{238}U. The elastic scattering peak (0^+) and inelastic scattering peaks corresponding to the first 2^+ (45 keV) and 4^+ (148 keV) states appear clearly in the spectra.

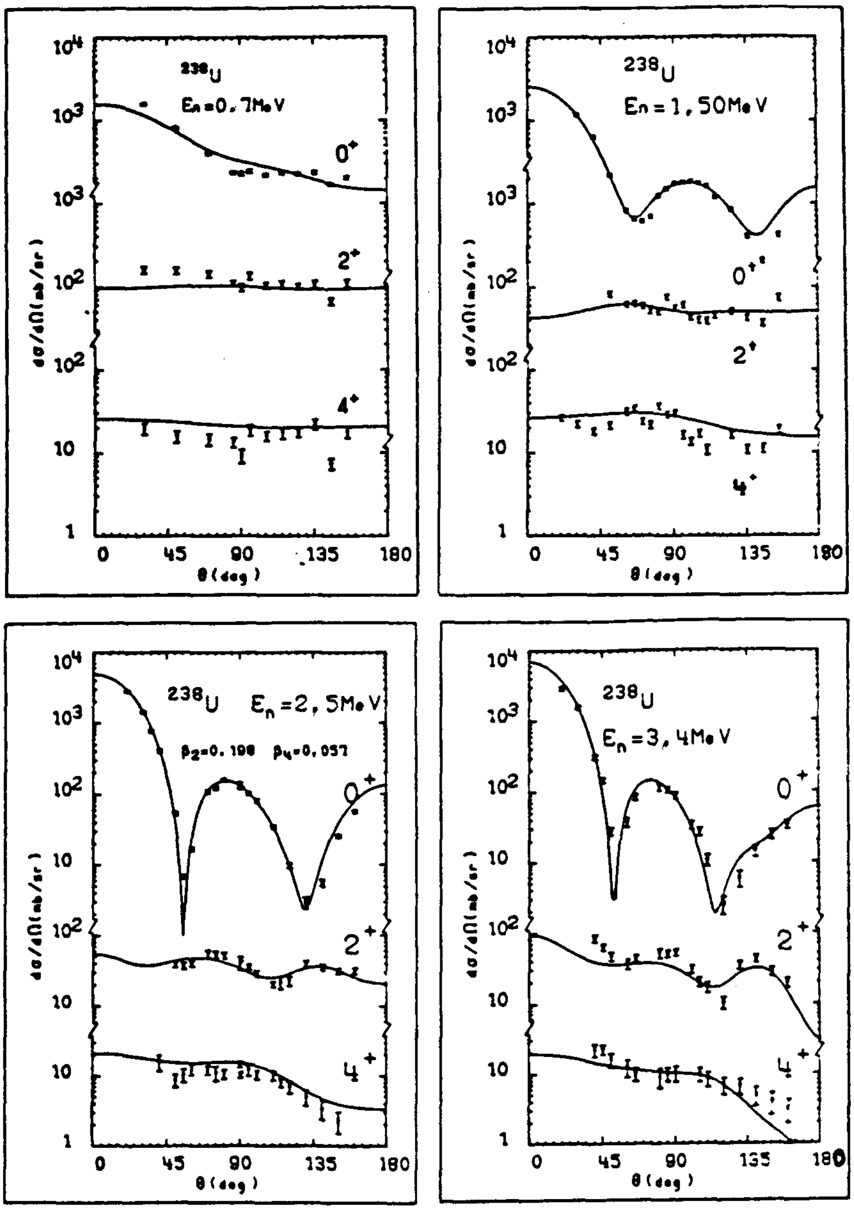

Fig. 2

Neutron cross sections at 0.7 - 1.5 - 2.5 and 3.4 MeV for the elastic scattering (0^+) and inelastic scattering to the first 2^+ (45 keV) and 4^+ (148 keV) states of ^{238}U.

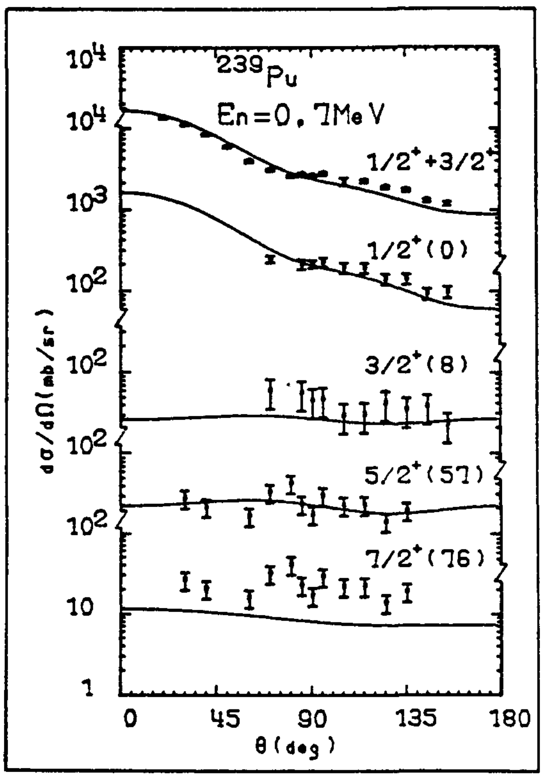

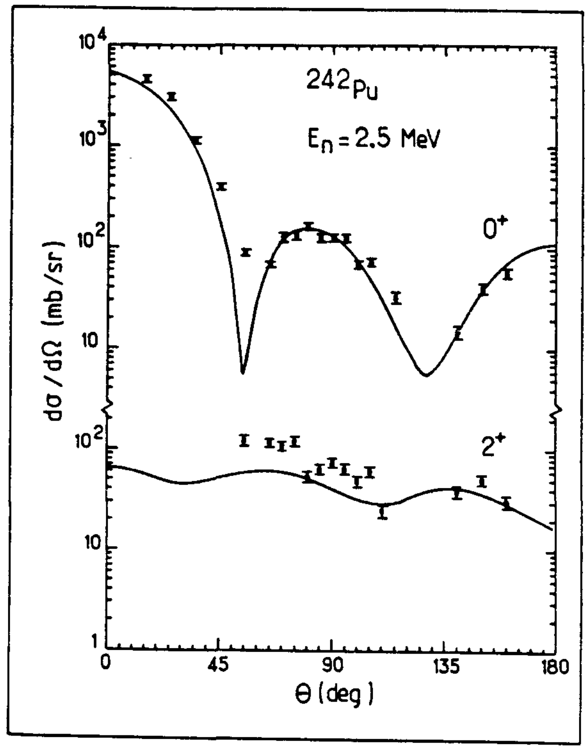

Fig. 3

Differential cross sections for ^{239}Pu at 0.7 MeV. The energy of the excited levels is given in keV.

Fig. 4

Neutron cross sections at 2.5 MeV for the elastic scattering (0^+) and inelastic scattering to the first 2^+ (44.5 keV) state of ^{242}Pu.

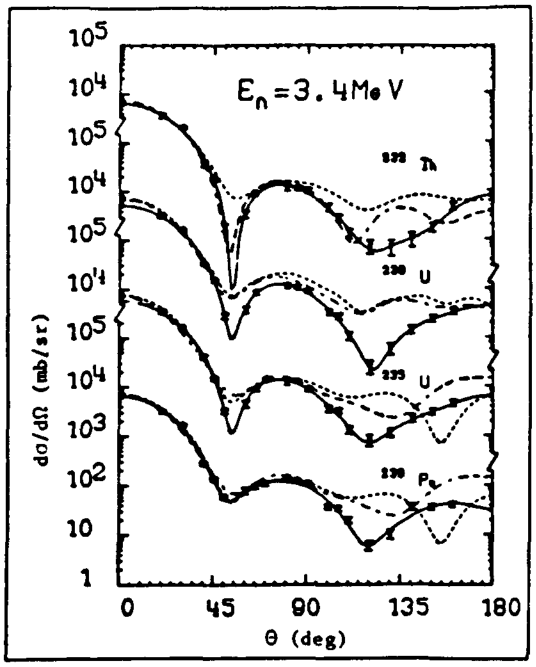

Fig. 5

Elastic scattering cross sections at 3.4 MeV for ^{232}Th and ^{238}U, and cross sections for the groups of levels ($7/2^-$, $1/2^+$, $3/2^+$) for ^{235}U and ($1/2^+$, $3/2^+$) for ^{239}Pu. Solid lines are coupled-channel calculations as described in the text. Dotted and dashed curves are angular distributions from the ENDF/B IV and ENDL 76 files respectively.

5/ THE $(n,\gamma f)$ REACTION IN SLOW-NEUTRON-INDUCED RESONANCES IN ^{239}Pu, ^{235}U and ^{241}Pu

J. Trochon, G. Simon

The $(n,\gamma f)$ reaction, a process resulting from competition between gamma ray emission and fission during de-excitation of a compound nucleus, has been studied in the resolved-resonance region for the target nuclei ^{239}Pu, ^{235}U and ^{241}Pu. It has been shown in reference [1] that all the experimental data reflect the effects of the $(n,\gamma f)$ reaction. Experimental values of the product $\Gamma_{\gamma f}.\bar{e}_{\gamma f}$ of the width of such a reaction and the mean value of the prefission gamma ray energy spectrum have been deduced. Then values of the width $\Gamma_{\gamma f}$ for the spin-parity $J\pi$ couples associated to "s-wave" incident neutrons have been derived from calculated values of the energy $\bar{e}_{\gamma f}$ and the experimental values of the products $\Gamma_{\gamma f}.\bar{e}_{\gamma f}$. The results are given in the table I. Details on the possible importance of the $(n,\gamma f)$ reaction will be found in reference [1] in regard of evaluating cross sections as well as studying fission barriers and class-II vibrational states.

Reference of chapter 5

[1] J. Trochon ; Physics and Chemistry of Fission 1979, Proceedings of a Symposium, Jülich 14-18 may 1979, IAEA Vienna, Vol. I (1980) p. 87.

TABLE I

Target nucleus	$J\pi$	$\Gamma_{\gamma f}.\bar{e}_{\gamma f}$ eV^2	$\bar{e}_{\gamma f}$ keV	$\Gamma_{\gamma f}$ meV
^{239}Pu	0+	8000±1900	1100±50	7.3±1.8
	1+	4600±300	1080±50	4.2±0.4
^{235}U	3-	4020±2030	850±50	4.7±2.3
	4-	1730±590	800±50	2.1±0.7
^{241}Pu	2+	6982±3819	800±100	8.7±4.9
	3+	1714±664	800±100	2.1±0.8

Characteristics of the (n,γf) reaction in slow-neuton-induced resonances in ^{239}Pu, ^{235}U and ^{241}Pu.

$\bar{e}_{\gamma f}$ = mean value of the prefission gamma ray energy spectrum (theoretical evaluation).

$\Gamma_{\gamma f}.\bar{e}_{\gamma f}$ = product of $\bar{e}_{\gamma f}$ by the width of the (n,γf) reaction (experimental evaluation).

6/ NEUTRON CROSS SECTIONS OF ^{231}Pa

(*S. Plattard, J. Jary (BRC) ; G.F. Auchampauh, N.W. Hill, G. de Saussure, R.B. Perez, J.A. Harvey (LASL)*)

The measurements of the ^{231}Pa fission cross section in the threshold region [1] show significant intermediate structures which were interpreted by Sicre [1] as due to vibrational states trapped in the second minimum of a double humped fission barrier of ^{232}Pa.

Meanwhile fine structures in the $^{230,232}Th$ fission cross sections were observed by Blons et al. [2] and attributed to members of rotational bands built on vibrational states (of same K and opposite parity) of an asymmetrically deformed third minimum of the fission barrier as predicted by Möller and Nix [3] for such light actinides. This situation should also apply to ^{232}Pa, and to investigate such a possibility a high resolution fission cross section measurement of ^{231}Pa was undertaken.

The Oak Ridge Electron Linear Accelerator (ORELA) was used as a neutron time-of-flight (TOF) spectrometer with a nominal resolution of 0.19 and 22 ns/m for experiments of Dubrovina and Muir respectively [1]. The experiment of Dubrovina was performed on a 42.7 m flight path which provided a resolution of 0.4 keV at a neutron energy E_n = 160 keV. The fission events were detected in a sealed gaseous scintillator containing 265 mg of ^{231}Pa in the form of 0.3 mg/cm^2 protactinium oxide layers [4]. A separate cell of the detector was loaded with 130 mg of ^{235}U in order to allow normalization of the ^{231}Pa data to the ^{235}U fission cross section derived from the version IV of the Evaluated Nuclear Data File (ENDF/B-IV). The experiment of Muir was carried out on a 18.3 m flight path with essentially the same setup. The ^{231}Pa TOF spectrum was normalized with respect to the ^{235}U TOF data around E_n = 13 eV providing directly a quantity which behaves, within a few percent, like $\sigma_f \sqrt{E_n}$ for $E_n <$ 100 eV.

Below 100 eV (Fig. 1), a number of fission resonances are observed for the first time except for the 4 resonances below 1.3 eV already reported by Leonard et al. [5]. The resonance energies are in a very good agreement with those given by Simpson et al. [6] in their total cross section measurement. However, we observe additional resonances above 15 eV. Rather than being clustered around definite energies as observed in several subthreshold cross sections [7], these resonances seem to be uniformly distributed, at least below 100 eV. Because of poor statistics, it is not possible at the present time to verify it this behaviour is similar in the keV region. The average fission width $<\Gamma_f>$ computed for those resonances below 15 eV, where no resonances are missed in the total cross section measurement, is 8 μeV, about 3 to 4 orders of magnitude lower than what is generally measured for fissile nuclei.

We would like to point out that the average fission width of the narrow resonances observed in the eV region is in good agreement with that calculated using the double-humped barrier parameters of Sicre [1]($<\Gamma_f>_{calc}$ = 7.7 μeV). This is an additional confirmation that the third minimum, for this mass region, is rather shallow (see Table 2). Such an agreement between the observed and calculated average fission width also suggests that the acquired fission strength of the eV resonances is not a result of coupling between class I and class II states but rather a result of direct penetration through the total fission barrier.

Figure 2 displays a detailed picture of σ_f between 0.12 and 0.45 MeV where spectacular fine structures are visible for the first time due to the substantial improvement of the energy resolution of this measurement. As a result, the shape of the sharp resonance at 157.6 keV with a FWHM of 2.9 keV is now better defined (peak/valley ratio $\simeq$ 13). In addition, the good energy resolution reveals the presence of other sharp resonances (at least two in the vicinity of E_n = 370 keV) and separates into several components the broad peaks located around E_n = 190 and 330 keV. Table 1 gives a preliminary list of the peak energies of σ_f together with K^π values given by Sicre [1].

From his fission fragments angular distribution on ^{231}Pa ($I^\pi = 3/2^-$), Sicre [1] concluded that the resonance at 156.7 keV was a pure vibrational state having $K^\pi = 3^+$, that is to say obtained with ℓ = 1 neutrons. The present high-resolution data proves this statement to be correct since a rotational band built on a $K^\pi = 3^+$ vibrational state requires $\ell \geqslant 3$ neutrons, therefore leading to undetectable peak cross section. In addition, assuming a rotational parameter $\hbar^2/2\mathcal{J}$ = 2 keV [4], members of such a band would be about 20 keV apart, a value much larger than the energy spread over which the resonance extends. A spacing of a few keV would require a moment of inertia $\mathcal{J}$ incompatible with a stable shape of the nucleus.

Since we adopt the model of an asymmetrically deformed third minimum, one should expect to find vibrational states of both parities as it can be checked by a WKB calculation [8]. We speculate that the resonance located at 173.3 keV could be a possible candidate for a $K^\pi = 3^-$ vibrational state. Indeed, 1) the peak cross section has a correct magnitude to be formed with ℓ = 2 neutrons, and 2) its separation from the 3^+ state (16.6 keV below) is compatible to what has been reported by Blons et al. [2] for ^{231}Th and calculated by Möller et al. [3] for this mass region.

In order to support such considerations, we have calculated, using the statistical model [9], a theoretical cross section with the form :

$$\sigma_f^{calc}(E) = \sum_{J\pi} \sigma_c(E,J,\pi) \frac{T_f(E,J,\pi)}{T_f^t + T_n^t + T_\gamma^t} \cdot F$$

where σ_c is the compound nucleus formation cross section for a state at excitation energy E, spin and parity (J,π) ; T_n , T_f and T_γ denote the transmission coefficients for neutron emission, fission and radiative capture respectively, and the superscript t stands for summation over all channels for each mode ; F is a level width fluctuation factor [10]. The neutron penetrabilities are derived from a coupled channel calculation [11]. The fission probabilities were obtained from an exact solution of the Schrödinger equation where damping has been included [12].

Table 2 lists a preliminary set of barrier parameters used to compute the theoretical cross sections displayed as a full line on Figure 3. The $J\pi = 3^+$ and 3^- resonances in the third well, at 156,7 keV and 173,3 keV respectively, are well reproduced. The broad resonance around E_n = 190 keV has been interpreted as a vibrational state ($K^\pi = 0^+$) trapped in the second well and slightly damped into the intrinsic states associated to this well. The fluctuations in σ_f superimposed to this broad resonance can be due to coupling between class III and class II states or between collective and intrinsic states. A fission channel analysis at higher energies (up to E_n = 2 MeV) is in progress. It will permit us to calculate all the important neutron cross sections (compound elastic and inelastic scattering, and radiative capture) in this energy range from 2 MeV to 12 MeV; (n,2n) cross sections are also planned to be calculated starting from a global adjustment to the fission cross section [13] we have just measured.

References of chapter 6

[1] S.M. Dubrovina, and V.A. Shigin ; Sov. Phys. Doklady 9, 579 (1964).

D.W. Muir, and L.R. Veeser , in Proceedings of the Conference on Nuclear Cross Sections and Technology, Knoxville, TN, March 15-17, (1971) p. 292.

A. Sicre, Ph. D. Thesis, University of Bordeaux (1976), Report CENBG 7603.

[2] J. Blons, C. Mazur, D. Paya, M. Ribrag, and H. Weigmann ; Phys. Rev. Lett. 41, 1281 (1978).

J. Blons, C. Mazur, and D. Paya ; Phys. Rev. Lett. 35, 1749 (1975).

[3] P. Möller, and J.R. Nix, in Proceedings of Physics and Chemistry of fission, IAEA Vienna 1974, I, p. 103.

[4] S. Plattard, G.F. Auchampaugh, N.W. Hill, G. de Saussure, R.B. Perez and J.A. Harvey, in Proceedings of Conference on Nuclear Cross Sections for Technology, Knoxville TN, October 22-26, 1979, to be published.

[5] B.R. Leonard, Jr., and R. Odegaarden ; Bull. Am. Phys. Soc. 6 8 (1961) ; Hanford Report 67219 (1960).

[6] F.B. Simpson, W.H. Burgus, J.E. Evans, and H.W. Kirby ; Nucl. Sci. Eng. 12, 243 (1960).

[7] D. Paya, H. Derrien, A. Fubini, A. Michaudon, and P. Ribon, in Nuclear Data for Reactors, IAEA Vienna 1967, II, p. 128 - A. Fubini, J. Blons, A. Michaudon, and D. Paya ; Phys. Rev. Lett. 20 1373 (1968).

E. Migneco, and J.P. Theobald ; Nucl. Phys. A112, 603 (1968).

G.D. James, J.W.T. Dabbs, J.A. Harvey, N.W. Hill, and R.H. Schindler ; Phys. Rev. C15, 2083 (1977).

F.C. Difilippo, R.B. Perez, G. de Saussure, D.K. Olsen, R.W. Ingle ; Nucl. Sci. Eng. 68, 43 (1978).

[8] L.D. Landau, and E.M. Lifshitz, in Quantum Mechanics, Pergamon Press (1958), p. 176.

[9] J. Jary ; Code NRLY (1977).

[10] P.A. Moldauer ; Nucl. Phys. 47, 65 (1963).

[11] Ch. Lagrange ; private communication.

[12] J. Guillot ; internal report P2N-914/80

[13] J. Jary ; report CEA-R-4647 (1975).

TABLE I

E_n(keV)	K^π	E_n(keV)	K^π
156.7	3^+	304.5	
173.3		312.1	
182.3		319.3	
187.4		328.6	0^+
193.8	0^+	336.7	
281.9		371.1	
300.6		375.7	

Resonance energies and corresponding K^π values

TABLE II

K^{π}	E_A	E_{II}	E_B	E_{III}	E_C	$\hbar\omega_A$	$\hbar\omega_{II}$	$\hbar\omega_B$	$\hbar\omega_{III}$	$\hbar\omega_C$
3^+	5.77	3.237	6.150	5.362	6.150	0.950	1.000	0.650	0.800	0.650
3^-	5.85	3.237	6.166	5.378	6.166	0.950	1.000	0.650	0.800	0.650
0^+	5.92	3.475	6.120	5.700	6.120	0.950	1.000	0.950	0.800	0.950

Fission barrier parameters (MeV)

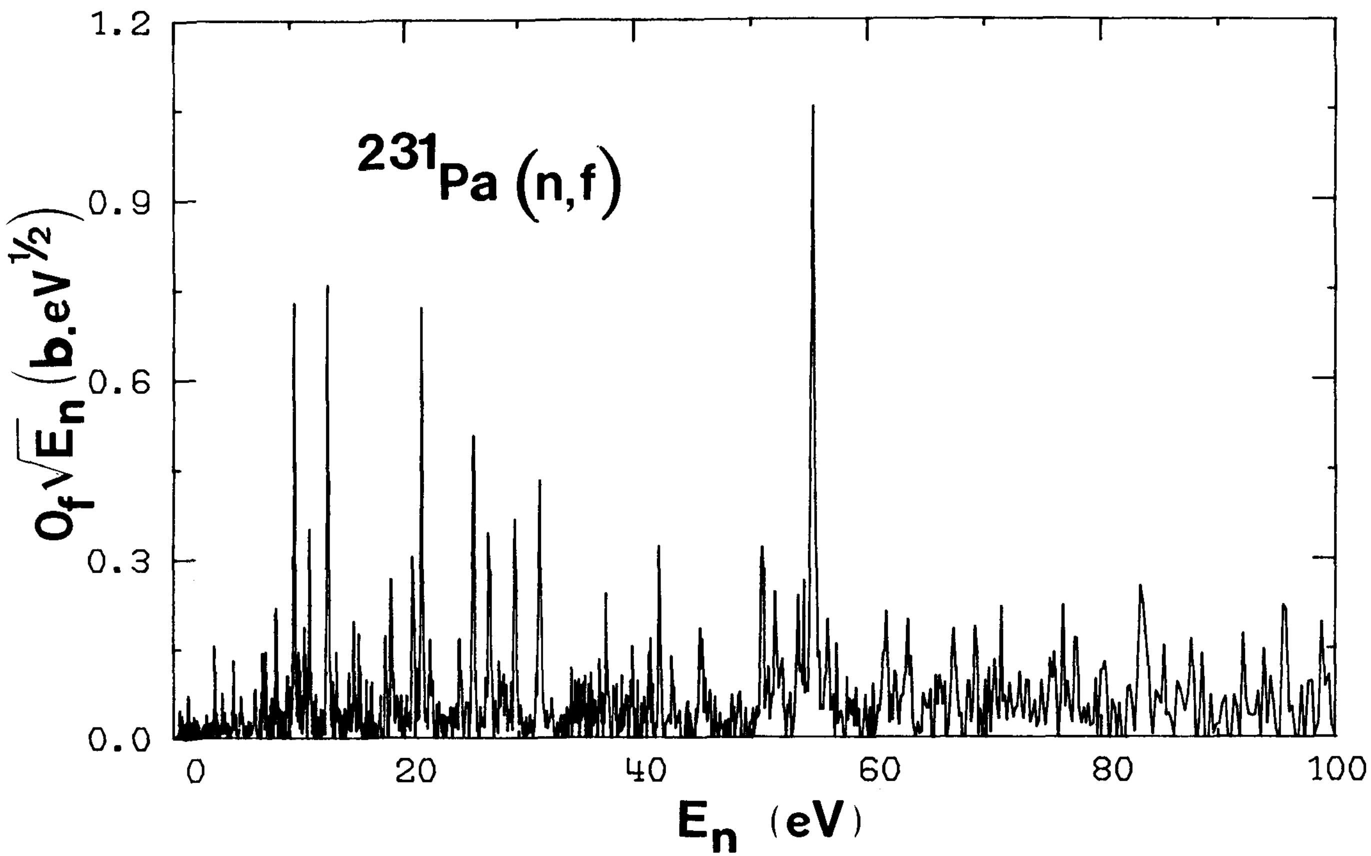

Fig. 1

Measured fission cross section of ^{231}Pa between 0.4 and 100 eV.

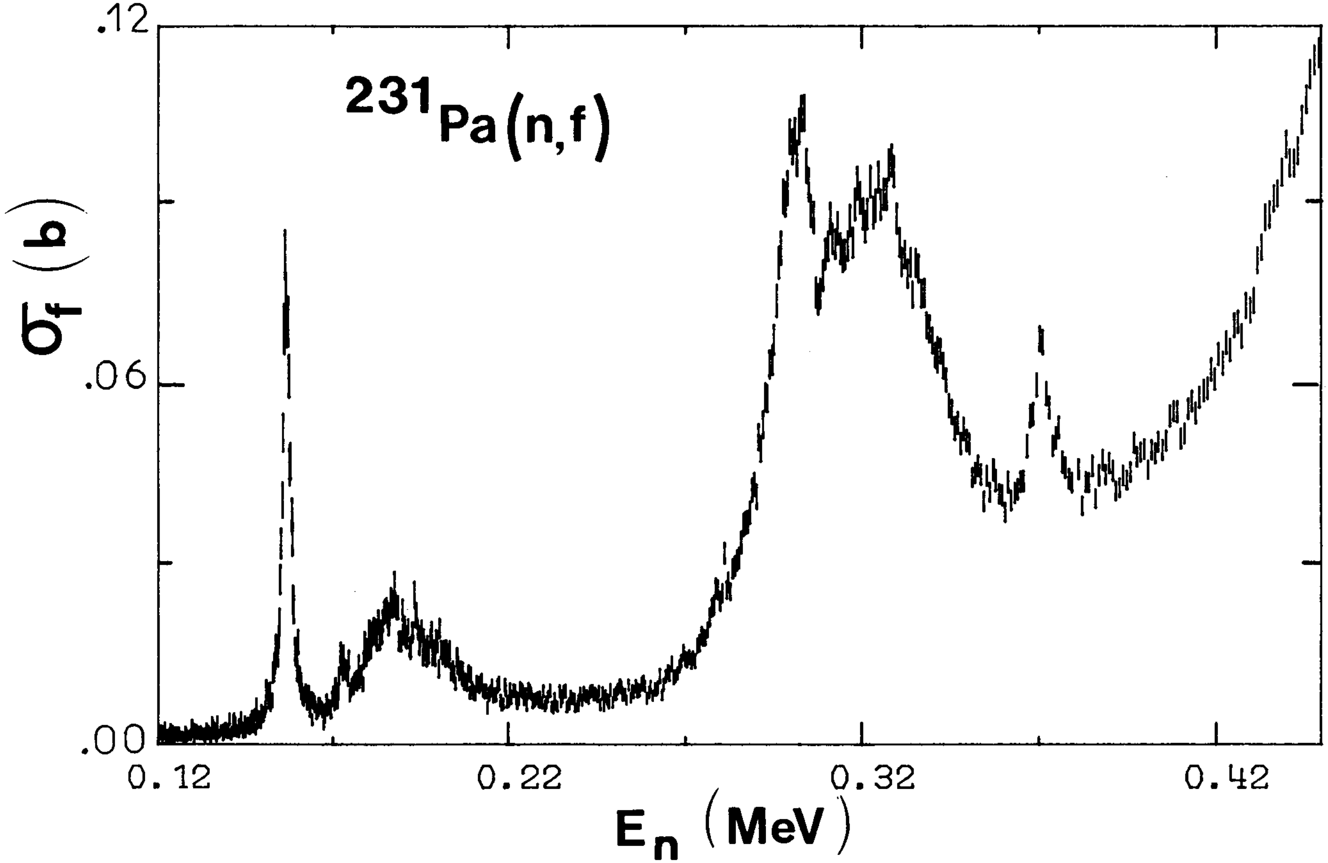

Fig. 2

Measured fission cross section of ^{231}Pa between 0.12 and 0.42 MeV.

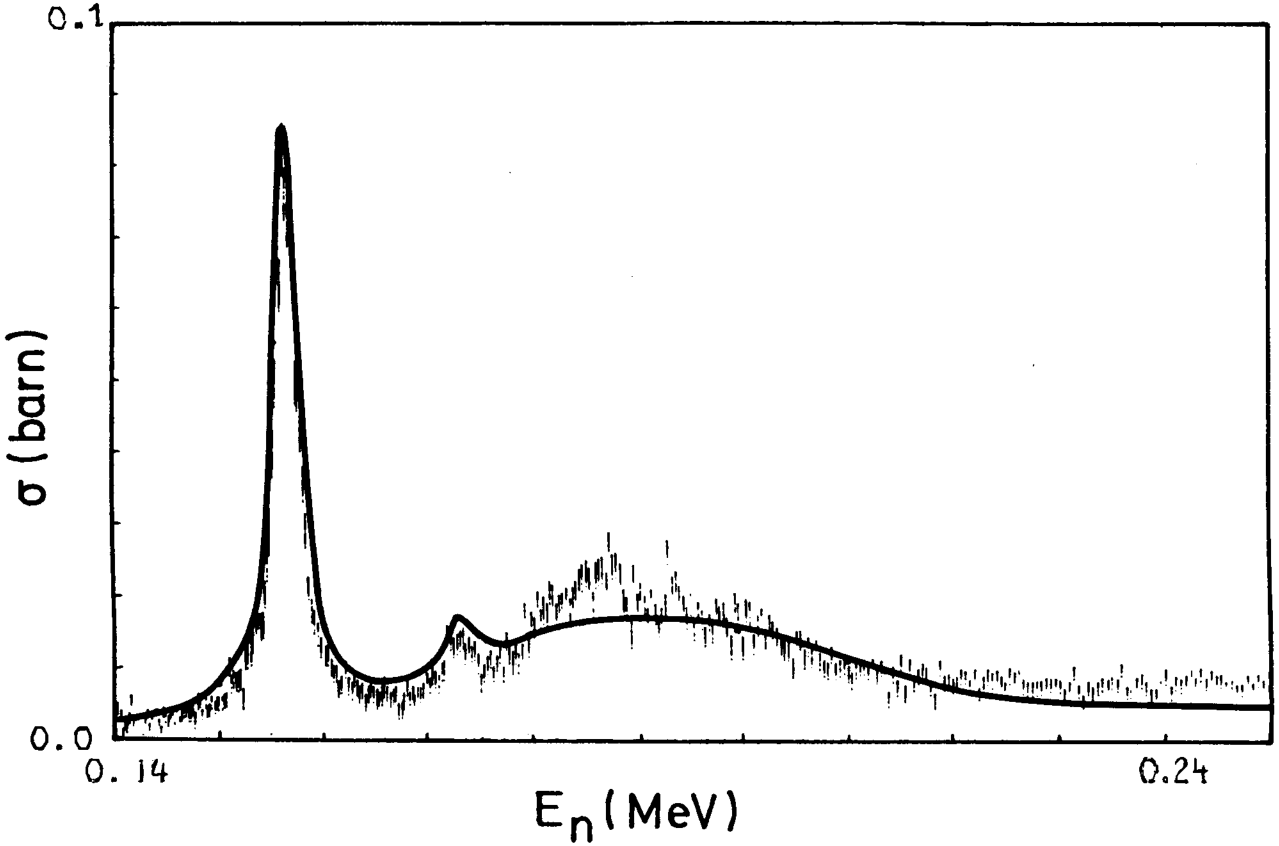

Fig. 3

Fission cross section of ^{231}Pa between 0.14 and 0.24 MeV. The solid line is a preliminary result of a fission channel analysis.

7/ SYNOPSIS : AN INTERACTIVE NUCLEAR DATA EVALUATION FILE INTERFACE AND MAINTENANCE SYSTEM

M. Collin, D. Cotten, C. Philis

7-1- INTRODUCTION

The information system SYNOPSIS was created at Bruyères-le-Châtel to handle the increasing number of requests for evaluated nuclear data. Each program in SYNOPSIS can store or retrieve, in a convenient form, data of several available evaluated data files (Figure 1).

The first step was to store on disk, using the smallest size, the various evaluated nuclear data libraries and to write programs which read in direct access any array (cross section versus energy for example) as fast as possible. This was accomplished by the original SYNOPSIS, described in Ref. [1]. It is summarized in the next paragraph. Following the first months of utilization, evaluators also wanted a storage system allowing direct access to variable experimental or computed data, and graphical display programs able to deal with both evaluated and experimental data.

We summarize hereafter the modifications which have introduced these above features after the publication of the first report [1].

These modifications were described at ICTP Trieste in february 1980.

7-2- BASIC PRINCIPLES

At present, SYNOPSIS consists of the two different subsystems RAPIDE and MINI.

The RAPIDE system allows us to store and read in direct access all of the nuclear evaluated data files. It is basically the original SYNOPSIS.

So we must optimize :

- minimum disk space used for a storage
- fast access to each data set
- updating facilities

We sequentially store on the file MEGA the data sets in binary format (to earn a factor greater than 3 in disk space). The size of this file (40 Mbytes) permits the storage of 1 600 000 cards (for example ENDF BIV = 300,000 cards).

The storage address and identification of section are stored on file DIM1 (DIM1 = DIrectory of MEGA n° 1).

A retake file REPR allows us to store evaluated data in several runs, this file containing the addresses of the first free space on MEGA and DIM1 files.

To increase the speed of access, we sort DIM1 according to Z, then A, MF, MT, library and version number.

The sorted file is called DIMT

A binary search on DIMT allows us to reach any of 32000 sections with only 15 accesses to DIMT.

Of course, this procedure requires that the first access to newley-stored data occurs after a new sort of DIM1, building a new DIMT.

A complete description of the storage procedure is given in the next paragraph.

The MINI system handles experimental or computed data, and is slightly different from RAPIDE in what follows :

- Data are stored for a short period of time and each data set must be read just after its storage, so that a procedure such as the creation of DIMT is avoided.

- Each user must handle his own data sets without disturbing the other user's data.

Fast access requires a small size for each user's index (now 120 sections maximum).

Comparison programs can access both the RAPIDE and MINI Systems.

Nature and format of the data sets stored in MINI can be very varied.

Each user can modify the content and the size of each of his stored data sets. During the first storage of a data set, the largest size which will be necessary must be defined with prudence in order to avoid wasted disk space.

7-3- STORAGE PROCEDURES

The differences between the RAPIDE and MINI systems oblige us to use different storage procedures

a) The RAPIDE storage procedure must permit

- storage of the data sets
- updating of the indexes
- the certainty that each identification of a section is unique. If

we detect two different addresses for a given section, we meet either a duplicate or a new version. Index files will be modified.

Thus the storage procedure in RAPIDE consists of

1 - The storage program

2 - Detection of isomers

3 - Sorting of DIM1 to built DIMT

4 - Detection of duplicates, using DIMT

If we meet duplicates :

5 - Modifications of DIM1 (Z number or version number)

6 - A new sorting to built the new DIMT

During the time needed for this procedure, it is always possible to use the RAPIDE system to treat the data sets sorted before the previous sorting.

In fact, the REPR file contains the size of the usable DIMT and this value is modified during step 4. So we can store (step 1) several data sets and begin steps 2 and 3, even if a user needs the old data sets.

b) The storage procedure on MINI is completely different, even if we also encounter a retake file, an index file and a storage file.

The index file is divided in 5 areas, one for each user, and each containing up to 120 sections. The access procedure has to read sequentially 120 values to reach a given data set.

The storage procedure assumes the following points :

If a new user must store his first data set, he uses the user number 0 and the program gives him the first free user number (up to 5).

After that, the program looks for the identification of the data set on the user index.

If it is found, the new data replaces the old one if the maximum size available permits it.

If not found, a new data set is created, a new index line written and we modify the retake file.

This procedure allows us to accept data sets having very different sizes, because the storage area is sequential and filled by the different users without waste of space.

7-4- UTILIZATION

We can use two kinds of programs.

The fist type accepts data sets read on the RAPIDE and MINI systems.

The second type consists of a program for editing evaluated data.

Some of the programs now in use are :

1 - SYLVIE program (SYnopsis, Lecture et VIsualisation) is an editing program which performs various functions :

. to visualize either evaluated or experimental data (size and type of coordinate axis can be chosen)

. to sample data set from each curve in order to build a private one

. to modify (addition, suppression or renormalization) the private one

. to store this data set on MINI system.

2 - The plot program to obtain one or several curves on the same graph on paper.

3 - Editing programs.

MATER copies the complete description of a given material in the original format.

FUMAT gives a partial description in the same format with update of the dictionary.

SORMT outputs one or several sections chosen in one or several libraries.

4 - Otherwise, if a program requires a large number of sections from one or several materials, we can modify it to reach them on the RAPIDE system.

7-5- CONCLUSION AND FUTURE PLANS

This system was built to be used with a mini computer. In particular, we developed it on a 16 bits word computer SEMS MITRA 125 and we met some difficulties because integer values cannot be greater than 32767.

The present version of SYNOPSIS is available on a 50 megabytes disk. It contains ENDF BIV, BV and ENDL as well.

But this size will become too small if we intend

. to store other libraries such as KEDAK
. to uptade the old data sets
. to store our own private library containing the results of our evaluations.

We are preparing the next series of routines to obtain :

. the treatment of spectra ; the present status of SYNOPSIS only permits us to handle tabulated cross sections.

. the tabulation of parametrized data by use of routines already written

. an editor to create a complete description of a material, gathering cross sections read either on RAPIDE or on MINI.

Such a description is being ready to be tested by CHECKER and PSYCHE.

Reference of chapter 7

[1] M. Collin, A. Schett, C. Philis ; Synopsis, an interactive nuclear data evaluation file interface and maintenance system. Part I : Basic concept. Report NEANDC(E) 207"L" ; INDC(FR) 37/L (January 1980).

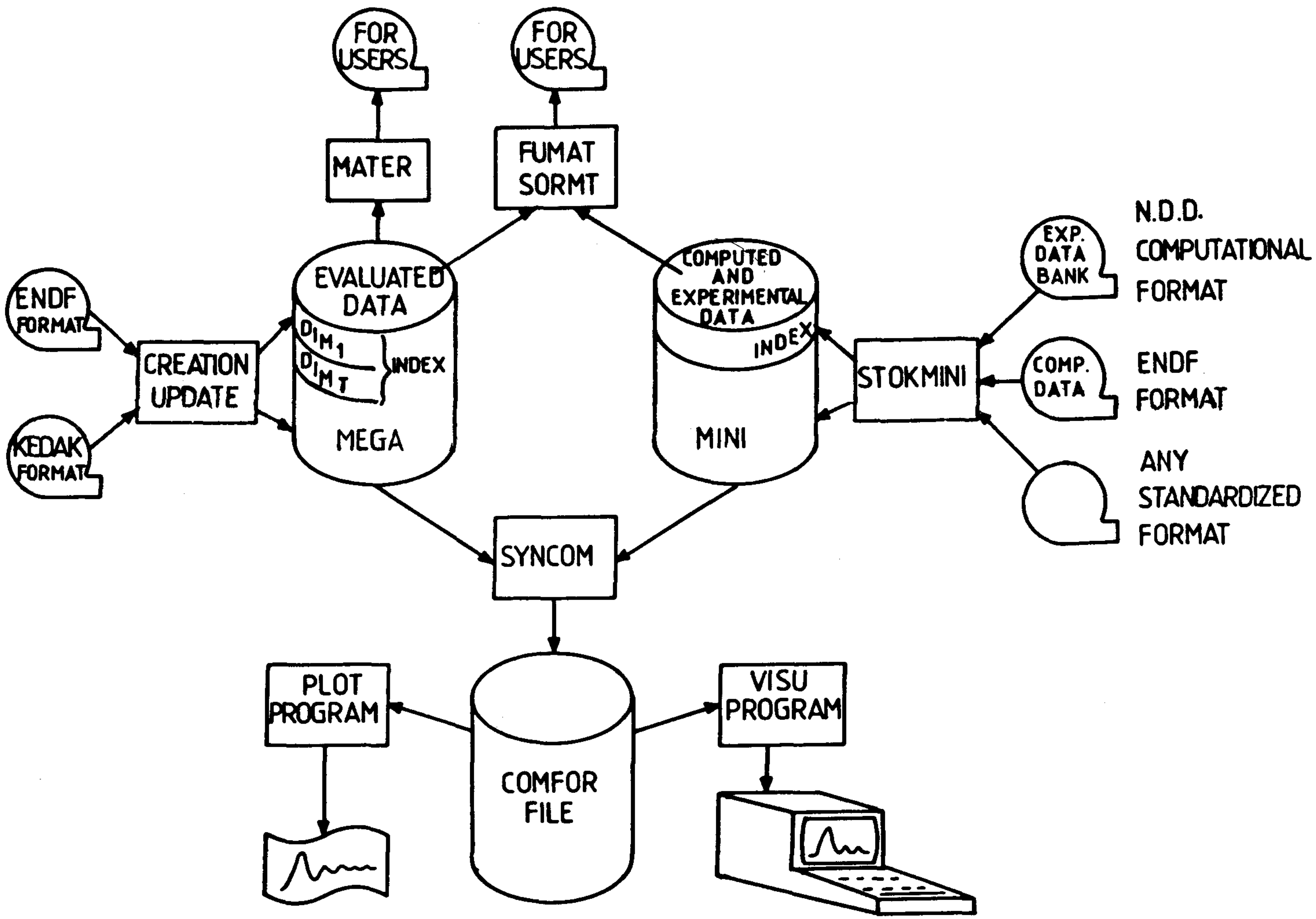

Fig. 1

Present development of Synopsis

8/ USE OF OPTICAL AND STATISTICAL MODELS FOR INTERPRETING ACTINIDE NEUTRON CROSS SECTIONS AT 0.7 MeV

J. Jary, Ch. Lagrange

Following the method described in reference [1], neutron cross sections (elastic, inelastic scattering and radiative capture) were calculated at .7 MeV by using optical and statistical models for ^{233}U, ^{235}U and ^{239}Pu.

The total, the shape elastic and direct inelastic scattering cross sections were obtained from a coupled-channel calculation in the frame of the "fictitious even-even nucleus" method [2]. The corresponding optical model parameters are given in reference [3].

The generalized neutron penetrabilities resulting from these calculations were introduced into our statistical model code which describes the compound nuclear reactions such as compound elastic and inelastic scattering, radiative capture and fission.

The fission barrier parameters of ^{240}Pu and ^{236}U derived from an adjustment to the corresponding ^{239}Pu and ^{235}U fission cross sections and fragment angular distributions between 10 keV and $\sim$ 60 keV are given in Table 1. In this energy range the scattering and radiative capture cross sections calculated using these parameters agree very well with the corresponding measured cross sections. Starting from the barrier shape of the $K^{\pi} = 0^{+}$ transition state given by Back [4], we obtain the same position for the $K^{\pi} = 0^{-}$ and $K^{\pi} = 2^{+}$ states, but band-heads with $K^{\pi} = 1^{-}$, 1^{+} and 2^{-} are necessary to obtain a good fit onto both fission cross sections and fission fragments anisotropies.

Some results concerning the scattering cross sections at 700 keV are given in reference [3].

References of chapter 8

[1] J. Jary, Ch. Lagrange, P. Thomet ; Report INDC(FR) 9/L - NEANDC(E) 174"L" (1977).

[2] Ch. Lagrange, O. Bersillon, this report (chapter 9).

[3] J. Lachkar et al. ; Report NEANDC(E) 201/L - INDC 32/L p. 50 (1979).

[4] B.B. Back et al. ; Phys. Rev. C9 (1974) 1924.

TABLE I

Compound nucleus	0^+ state						ΔE (MeV)				
	E_A	$\hbar\omega_A$	E_2	$\hbar\omega_2$	E_B	$\hbar\omega_B$	0^-	1^-	1^+	2^-	2^+
^{240}Pu	5.8	0.82	2.4	1.0	5.45	0.6	0.6	0.3	1.050	0.750	0.400
^{236}U	5.7	0.9	2.7	1.0	5.68	0.5	0.150	0.450	1.050	0.850	0.180

Fission barrier parameters

The energies are in MeV. The ΔE values give the position of the different band-heads of the transition states with respect to the 0^+ state.

9/ COUPLED CHANNEL OPTICAL MODEL CALCULATIONS FOR EVALUATING NEUTRON CROSS SECTIONS FOR ODD-MASS ACTINIDES

Ch. Lagrange, O. Bersillon

The purpose of this work is to investigate a simple collective model for evaluating neutron cross sections : total, direct elastic and inelastic cross sections as well as transmission coefficients needed in statistical model calculations for odd-mass actinide nuclei. As a matter of fact these deformed nuclei are relevant to coupled channel calculations as pointed out many years ago by Bohr and Mottelson [1]. Such a formalism was presented in detail by Tamura [2] and the notation used below follows the convention used by this author. To carry out properly the calculations many states have to be coupled in, leading to an outrageous computing time.

Let us consider the case of a system involving a target ground state I_o and n states coupled in with spin I_n, a projectile of spin s (s = 1/2) with a maximum value of the angular momentum j_{max}. For a given set of the angular momentum and parity of the whole system $J\pi$ the number of coupled equations N_i associated with the i^{th} target state is equal to $2I_i + 1$. The time needed to solve a set of N coupled equations system, where $N = \sum_{i=1}^{n} N_i$, is proportional to N^3. Moreover this set has to be solved J_{max} times (with $J_{max} = I_o + j_{max}$). Thus the computing time is roughly proportional [2] to the factor $J_{max}\ N^3$. Calculations of this factor for even and odd-mass nuclei are presented in Table I, using various coupling schemes, in the case of $j_{max} = 11/2$. For clarity these comparisons are relative to the typical case of an even-mass nucleus and a [0^+, 2^+, 4^+] coupling scheme. This coupling scheme has been found [3] to be more convenient than a [0^+, 2^+] one to reproduce the experimental data of ^{238}U. These results clearly show that the coupling scheme to be chosen is a crucial point in the determination of the machine time needed for calculations.

It can be thought that the parameterisation obtained for neighbouring even-A nuclei (for example ^{232}Th, ^{238}U) can serve as a guide for the odd-A ones (for example ^{235}U). So, we shall attempt to discover a model which would permit to extrapolate from the even to the odd-mass nuclei, and reduce considerably the computing time.

One of the most obvious procedures is based on the use of the adiabatic approximation in the coupled channel calculations (ACC). It has the advantage that the coupling to all the ground band states is automatically included. But the ACC approximation can be applied with confidence only when the energy of the projectile is in principle much higher than the excitation energies of the states mentioned above. Thus this approximation is not appropriate for the determination of a coherent optical parameter set needed for neutron cross section calculations in the full energy range 10 keV - 20 MeV. A convenient solution should be to use non-adiabatic coupled channel calculations (NACC) for the lower energies and ACC calculations at higher energies. But as it can be seen in Table 2, the matching energy between these models is not yet obtained at E_n = 3.4 MeV. Other calculations, not presented for brevity here, show that a very good agreement between both calculated results is obtained at a projectile energy of about 10 MeV. It is however clear that this matching energy could be smaller if the coupling scheme used in NACC calculations is increased (for example a coupling up to the $11/2^+$ or $13/2^+$ in the case of ^{239}Pu), but the machine time, needed for NACC calculations, would be then prohibitive. For these reasons we present and test another model that we call "the fictitious even-even nucleus" model.

This model consists in performing NACC calculations for an odd-mass nucleus by assuming a fictitious ground state rotational band (for example : 0^+, 2^+, 4^+). A simple method was proposed by D. Madland [5] to calculate the excitation energies of this "fictitious nucleus" ground state rotational band. The method consists in determining the moment of inertia and the single particle energy for the actual nucleus and using them for obtaining the excited states of the fictitious even-even nucleus. Such a method was employed here for the evaluation of ^{241}Pu neutron cross sections (cf. chapter 10). A more crude method was employed, as a test, for ^{239}Pu : in this method the excitation energies of the fictitious ground state band were interpolated from the neighbouring even-even isotopes. The direct cross sections for the transition from the ground state (I_0) to an excited state (I_i) of the odd-A nucleus are expressed in terms of the direct cross sections obtained for the "fictitious" 0^+, 2^+, 4^+ states as follows :

$$\frac{d\sigma}{d\Omega}(I_i) = \sum_{\lambda=0,2,4} \langle I_0\ \lambda\ K0 | I_i\ K\rangle^2 \frac{d\sigma}{d\Omega}(\lambda^+) \tag{1}$$

where K is the Z'-projection of the angular momentum of the last nucleon for the odd-A nucleus. It is worth while to note that the flux is conserved if the assumed coupling scheme for the odd-A nucleus is the following one :

$$I_0,\quad I_0+1,\quad I_0+2,\quad I_0+3,\quad I_0+4 \tag{2}$$

Comparisons of results obtained using this "fictitious even-even nucleus" model and the actual coupling scheme as defined by Eq. (2) are presented in Table 3 : for ^{239}Pu (K = 1/2), and in Table 4 : for ^{241}Pu (K = 5/2). These calculations were performed, in order to reduce the computing time, assuming a projectile spin equal to zero and the deformation and optical model parameters given in Chapter 10. In these calculations, as in the case of even-A nuclei, quadrupole and hexadecapole deformations are taken into account and the optical potential is expanded in Legendre polynomials up to an order equal to 8.

As can be seen from Table 3 there is for ^{239}Pu a general very good agreement between the two models employed. This good agreement is met in the case of ^{241}Pu only for a projectile energy equal or greater than 4.0 MeV. Comparisons of the direct inelastic scattering cross sections using both models are shown for ^{241}Pu in Fig. 1 and 2. We have chosen to present these cross sections only for the $7/2^+$ and $11/2^+$ states as examples, but the agreement is comparable for the $9/2^+$ and $13/2^+$ states. In the case of ^{239}Pu the results obtained using both models cannot be by eye differencied.

Transmission coefficients are needed for estimating some neutron cross sections using statistical model calculations. These transmission coefficients could be obtained in the frame of NACC calculations by using the following formula :

$$T^{J\pi}_{\ell j I} = 1 - \sum_{\ell' j' I'} \left| S^{J\pi}_{\ell j I,\ \ell' j' I'} \right|^2 \qquad (3)$$

From Eq.(3) it can be seen that the transmission coefficients obtained for odd-A nuclei depend on the angular momentum J of the compound system. In order to avoid this J dependence which is not taken into account in usual statistical model codes these coefficients can be compacted following :

$$T^{\pi}_{\ell,jI} = \sum_{J} \frac{(2J + 1)}{(2I + 1)(2j + 1)} T^{J\pi}_{\ell jI} \qquad (4)$$

Comparisons of neutron transmission coefficients calculated for the ground state using the actual coupling scheme and following Eq. (4) on one hand, and the "fictitious even-even nucleus" on the other hand, are presented for ^{239}Pu and ^{241}Pu in Tables 5 and 6 respectively. The agreement between the two kinds of calculations is similar to the one observed above for the cross sections.

The fact that the "fictitious even-even" model gives a good agreement with realistic calculations over the full energy range in case of ^{239}Pu (K = 1/2) and in a limited energy range in case of ^{241}Pu (K = 5/2) can be explained by the following consideration. The diagonal potential for the ground state of an even-A nucleus is defined as :

$$V_{g,s}(r) = V_{\lambda=0}(r) \cdot g_\lambda , \qquad (5)$$

whereas for an odd-mass nucleus :

$$V_{g,s}(r) = \sum_{\lambda=0}^{2I_0} \langle I_0 \| Q_\lambda \| I_0 \rangle \, g_\lambda \, V_\lambda(r) \qquad (6)$$

In these expressions the g_λ are geometrical coefficients (cf Ref.[2]), V_λ corresponds to the term of order λ in the Legendre expansion of the optical potential and the bracket is a reduced matrix element. Except for the case of I_0 = 1/2 the definition of the diagonal potential for odd-A nuclei is not the same than for even-A nuclei, and then the results obtained using the same set of parameters and eq.(5),(6) are different. Nevertheless the effect of that "reorientation" matrix element for the ground state of the odd-mass nuclei decreases as the projectile energy increases as clearly shown by our calculations.

We have presented a simple collective model for calculating neutron cross sections for odd-A nuclei. This "fictitious even-even nucleus" model needs less computing time than more realistic models. It can be applied as shown above with great confidence over the full energy range in the case of a ground state band K = 1/2. Moreover we think that this model can also be used in cases of a ground state band K ≠ 1/2 for the following reason. The experimental data (total cross sections, strength functions) used mainly for an optical parameter set determination do not differ greatly going from odd-A nuclei (^{233}U, ^{235}U) to even A nuclei (^{232}Th, ^{238}U, ^{242}Pu). Thus adjustments on these experimental data performed using NACC calculations with a realistic coupling scheme or a fictitious one would lead to different optical model parameter sets, but to the same calculated data. Because of that, the proposed model could be used over the full energy range.

Part of this work was completed at Los Alamos Scientific Laboratory by one of us (Ch. Lagrange). Useful discussions on the subject presented here with Dr. D. Madland are gratefully acknowledged. This research was supported in part by the United States Department of Energy.

References of chapter 9

[1] A. Bohr, and B.R. Mottelson ; Mat. Fys. Med. 27 n° 16 (1953)

[2] T. Tamura; Rev. Mod. Phys. 37 (1965) 679.

[3] Ch. Lagrange ; Acta Phys. Slov. 26 (1976) 32.

[4] G. Haouat et al. ; This report (Chapter 4).

[5] D. Madland ; (private communication).

I_0	0		1/2		5/2	
Coupling scheme	0,2	0,2,4	1/2,3/2 5/2	1/2,3/2 5/2,7/2 9/2	5/2,7/2 9,2	5/2,7/2 9/2,11/2 13/2
$\dfrac{N^3\ J_{max}}{x}$ (x = 18 562.5)	0.045	1.0	0.56	7.10	5.96	53.9

TABLE I - Rough evaluation of machine time needed for the coupled channel calculations (j_{max} = 11/2).

	σ_{tot} (barn)	σ_{reac} (barn)	$\sigma_{(1/2^+)}$ (barn)
A.C.C.	7.847	3.605	4.242
N.A.C.C. 1/2,3/2,5/2,7/2,9/2	7.983	3.627	4.356

TABLE II - Neutron cross section calculations for ^{239}Pu at E_n = 3.4 MeV. The optical model and deformation parameters are from Ref. 4.

	1.0 MeV		4.0 MeV		6.0 MeV	
	real	fict	real	fict	real	fict
σ_{tot}	7.079	7.069	7.797	7.796	6.943	6.942
σ_{CN}	3.472	3.475	3.1236	3.1235	2.991	2.991
$\sigma_{1/2^+}$	3.317	3.309	4.249	4.247	3.628	3.627
$\sigma_{3/2^+}$	0.09276	0.0872	0.1233	0.1232	0.09252	0.09252
$\sigma_{5/2^+}$	0.1281	0.1309	0.1845	0.1847	0.13875	0.13878
$\sigma_{7/2^+}$	0.03359	0.02979	0.0522	0.03168	0.04144	0.04126
$\sigma_{9/2^+}$	0.03569	0.0372	0.0644	0.0646	0.05157	0.05157

	10 keV	
	real	fict
σ_{tot}	16.392	16.384
σ_{CN}	5.476	5.468
$\sigma_{1/2^+}$	10.915	10.915
$\sigma_{3/2^+}$	0.00001	0.0

TABLE III - Comparisons of ^{239}Pu neutron cross sections (in barn) obtained from conventional (real) and "fictitious even-even nucleus" (fict) coupled channel calculations.

	1.0 MeV		4.0 MeV		6.0 MeV	
	real	fict	real	fict	real	fict
σ_{tot} b	7.0031	7.2940	7.821	7.831	7.0205	6.9918
σ_{CN} b	3.1887	3.5761	3.1713	3.1202	3.0749	3.0058
$\sigma_{5/2^+}$ b	3.6265	3.4888	4.3430	4.3976	3.7201	3.7203
$\sigma_{7/2^+}$ mb	135.48	123.11	153.27	165.99	116.94	126.80
$\sigma_{9/2^+}$ mb	38.088	68.79	86.395	75.09	60.80	75.05
$\sigma_{11/2^+}$ mb	14.30	42.21	41.750	67.37	29.71	34.25
$\sigma_{13/2^+}$ mb	5.965	7.350	26.834	11.70	18.03	9.44

TABLE IV - Comparisons of ^{241}Pu neutron cross sections (in barn) obtained from conventional (real) and "fictitious even-even nucleus" (fict) coupled channel calculations.

	1.0 MeV		4.0 MeV		6.0 MeV	
	real	fict	real	fict	real	fict
$\ell = 0$	0.53781	0.53825	0.59687	0.59729	0.65581	0.65590
$\ell = 1$	0.77064	0.77106	0.77764	0.77784	0.82406	0.82408
$\ell = 2$	0.28693	0.28735	0.54789	0.54831	0.63627	0.63637
$\ell = 3$	0.12568	0.12573	0.89228	0.89240	0.87728	0.87734
$\ell = 4$	$0.79967\ 10^{-2}$	$0.80096\ 10^{-2}$	0.37931	0.37962	0.61368	0.61383
$\ell = 5$	$0.59253\ 10^{-3}$	$0.5923\ 10^{-3}$	0.28233	0.28222	0.51840	0.51844
$\ell = 6$	$0.18130\ 10^{-5}$	$0.182\ 10^{-5}$	$0.30202\ 10^{-1}$	$0.30246\ 10^{-1}$	0.22226	0.22220

For E_n = 10 keV

$T_0 = 0.71891\ 10^{-1}$ (real)

$T_0 = 0.71890\ 10^{-1}$ (fict)

$T_1 = 0.35769\ 10^{-3}$ (real)

$T_1 = 0.35411\ 10^{-3}$ (fict)

TABLE V - Comparisons of ^{239}Pu neutron transmission coefficients obtained from conventional (real) and "fictitious even-even nucleus" (fict.) coupled channel calculations.

	1.0 MeV		4.0 MeV		6.0 MeV	
	real	fict	real	fict	real	fict
ℓ = 0	0.54276	0.54659	0.60757	0.59056	0.67796	0.66357
ℓ = 1	0.68069	0.79068	0.78757	0.78278	0.82935	0.82705
ℓ = 2	0.27691	0.29764	0.55997	0.54358	0.64457	0.6371
ℓ = 3	0.10973	0.12956	0.89182	0.89135	0.87509	0.8737
ℓ = 4	0.68641 10^{-3}	0.8582 10^{-3}	0.39983	0.38286	0.63585	0.6209
ℓ = 5	0.58808 10^{-4}	0.627 10^{-4}	0.281482	0.27895	0.51400	0.5133
ℓ = 6			0.31978 10^{-1}	0.30614 10^{-1}	0.2400	0.2304

TABLE VI - Comparisons of ^{241}Pu neutron transmission coefficients obtained from conventional (real) and "fictitious even-even nucleus" (fict) coupled channel calculations.

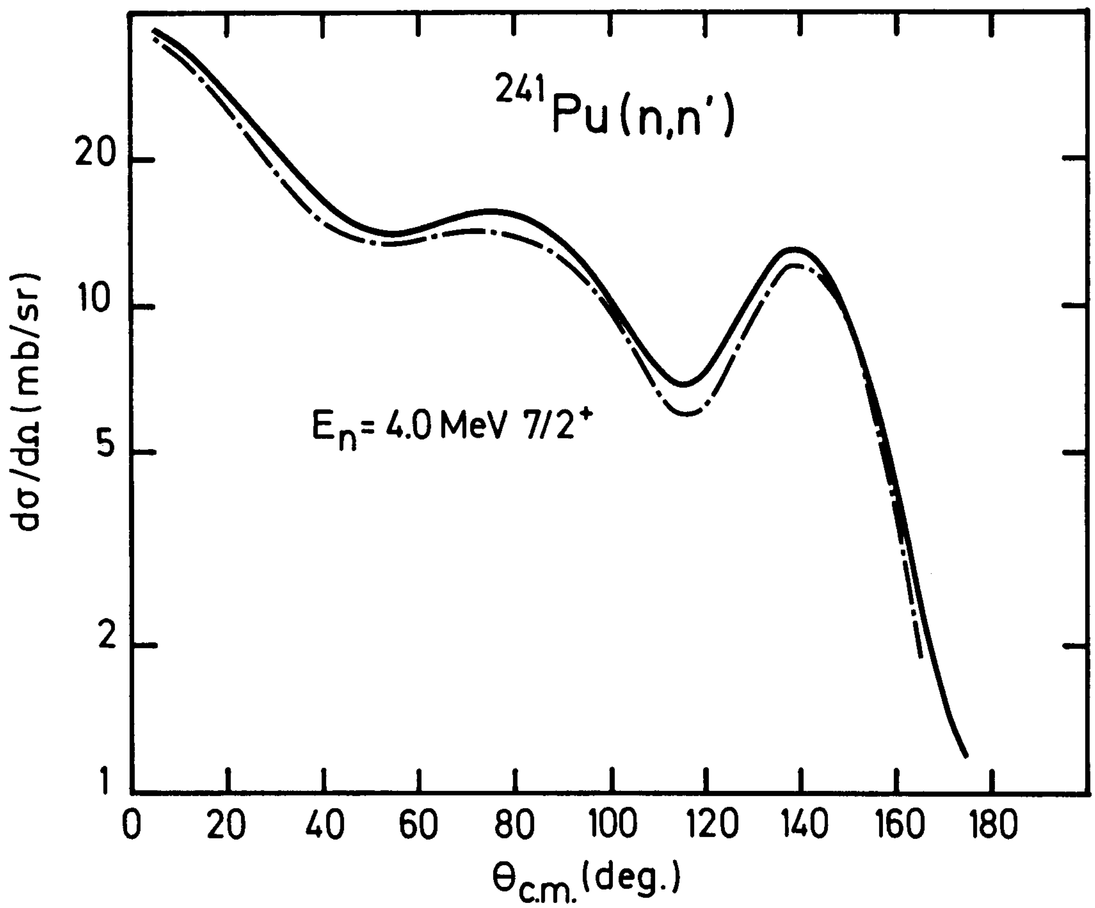

Fig. 1

Direct inelastic scattering cross section from the $\frac{7}{2}^+$ excited state of ^{241}Pu.

—— Conventional coupled channel calculation.

— · — "fictitious even-even nucleus" coupled channel calculation.

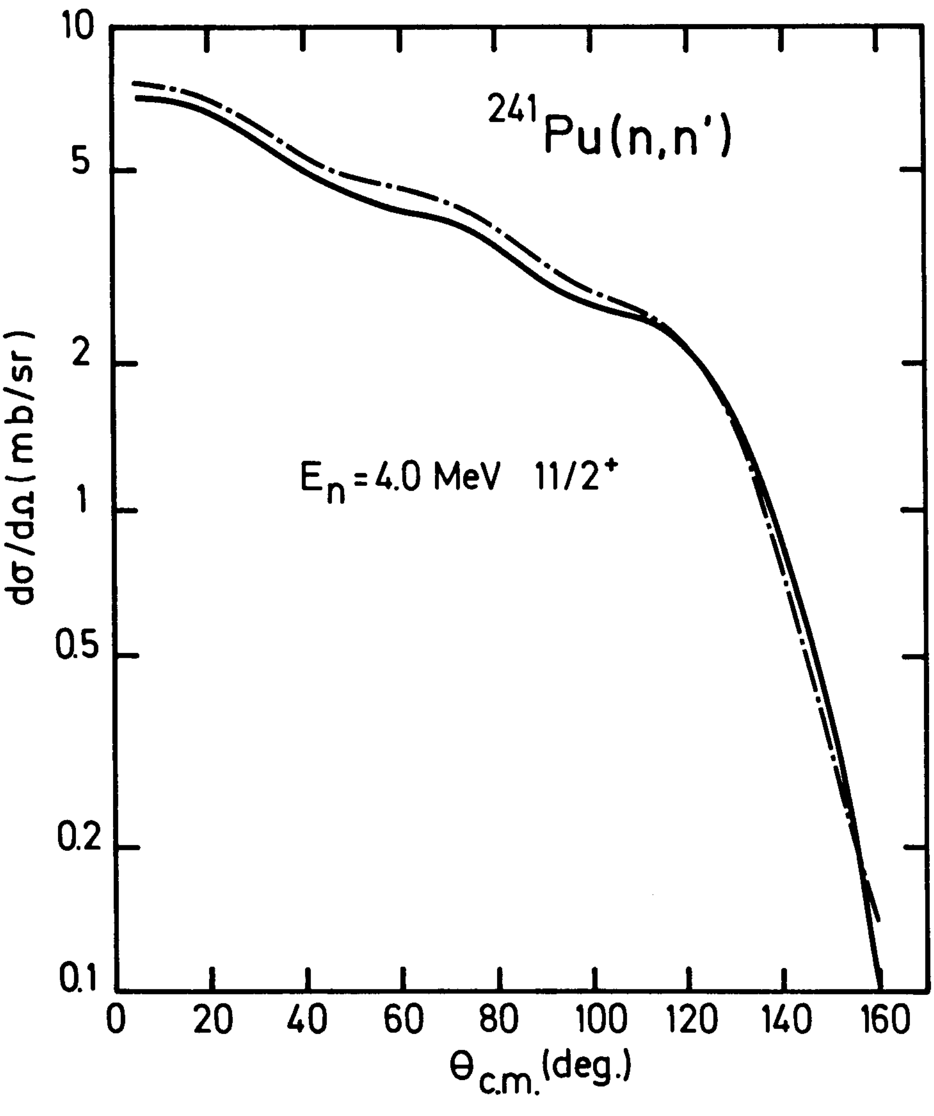

Fig. 2

Direct inelastic scattering cross section from $\frac{11}{2}^+$ excited state of ^{241}Pu.

—— conventional coupled channel calculation.

—·— "fictitious even-even nucleus" coupled channel calculation.

10/ EVALUATION OF NUCLEAR DATA FOR ^{241}Pu IN THE NEUTRON ENERGY RANGE FROM 10 keV TO 20 MeV

(Ch. Lagrange, O. Bersillon (BRC); D. Madland (LASL))

As no experimental measurements exist for many ^{241}Pu neutron cross sections, this evaluation is based on results obtained from nuclear models. Statistical model calculations are being performed using the code COMNUC-V of LASL. The fission channel barrier parameters of B.B. Back et al. [1], the average gamma width and observed level spacing from Ref. [2], and the discrete level scheme based on the work of Elze and Huizenga [3] are used. The transmission coefficients needed are obtained from a coupled channel (C.C) calculation which has been judged to be adequate to describe the ^{241}Pu neutron interaction cross sections. The C.C. optical model parameters have been determined so as to fit recommended values of the s-and p-wave strength functions [4], and the total cross section of the neighbouring nucleus ^{242}Pu [5]. The optical model parameters are presented in Table 1. Following a suggestion of Nix [6], the values of the deformation parameters (β_2,β_4) were obtained from an average between calculated values [6] for ^{242}Pu and ^{240}Pu. The optical model calculations have been performed using the "fictitious even-even nucleus" method [7]. One of us (D.M.) has determined a simple method by which the excitation energies of a "fictitious even-even nucleus" ground state rotational band can be determined for an odd-A deformed nucleus. The excitation energies so calculated are the followings : $E(2^+) = 0.0358$ MeV and $E(4^+) = 0.119$ MeV. The agreement obtained with the evaluated [8] low energy neutron data S_0, S_1, R' is reported in Table II. We present on Fig. 1 the calculated values of the total cross section together with the evaluation made by Konshin et al. [9], and the values deduced from ENDF/BIV [10]. A special attention has been paid to the direct excitation of the ground state rotational band. The corresponding direct inelastic scattering cross section has been found to reach about 300 mb near 4 MeV neutron incident energy.

References of chaper 10

[1] B.B. Back et al. ; Phys. Rev. C10 (1974) 1948.

[2] BNL-325, Third edition, Vol. 1 - INDC(USA)-58/L (1973).

[3] Th. W. Elze, J.R. Huizenga ; Phys. Rev. C3 (1971) 234.

[4] E. Menapace, M. Motta, A. Ventura ; report RT/FI (79) 5.

[5] M. Moore et al. ; contribution to the Knoxville Conference (1979).

[6] R. Nix ; private communication.

[7] Ch. Lagrange, O. Bersillon ; contribution to this Progress Report (chapter 9)

[8] E. Menapace et al. ; CNEN report n° 2114/CF (1979).

[9] V.A. Konshin et al. ; report INDC(CCP)-142/GJ (IAEA translation, 1980).

[10] ENDF/BIV, MAT = 1266.

TABLE I

Real central	Volume imaginary	Surface imaginary	Spin-orbit
$V = 46 - 0.27E$	$W_v = + 0.12E$	$W_D \begin{cases} = 3.3+0.35E & E \leqslant 8 \text{ MeV} \\ = 6.58-0.06E & E \geqslant 8 \text{ MeV} \end{cases}$	$V_{so} = 0.0$
$r = 1.26$, $a = 0.63$	$r = 1.26$, $a = 0.63$	$r = 1.26$, $a = 0.520$	

Optical model parameters. Geometrical parameters are expressed in fm, while the potential depths and incident projectile energy (E) are in MeV.

TABLE II

	S_0	S_1	R'
Evaluation (Ref. 8)	1.18	2.2	9.6
Calculation	1.12	2.36	9.26

Neutron strength functions (S_0,S_1) and scattering radius (R') for ^{241}Pu. The units are 10^{-4} $eV^{-1/2}$ for S_0 and S_1 and fermi for R'.

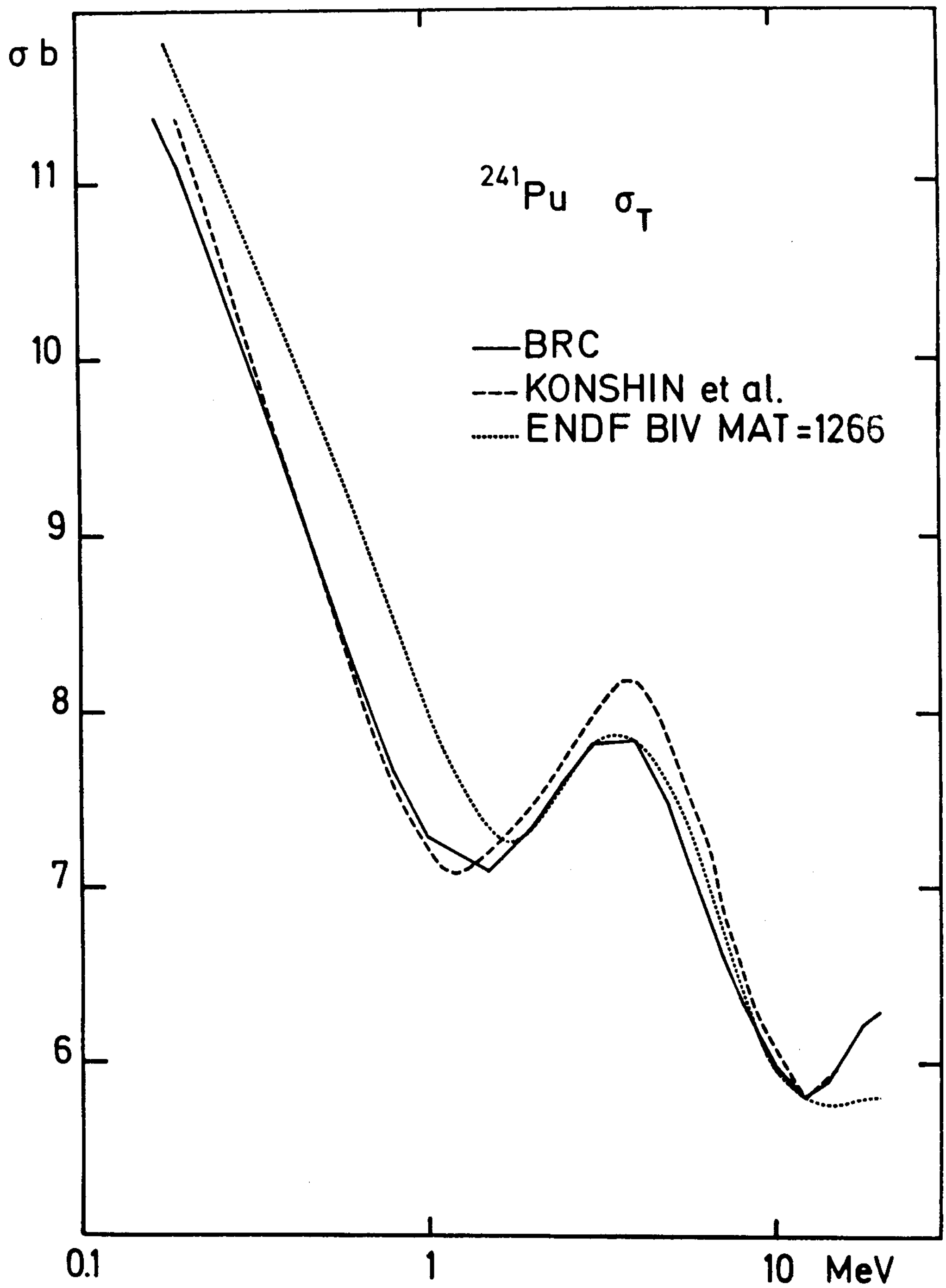

Fig. 1

Evaluated (Ref. 9,10) and calculated neutron total cross sections for ^{241}Pu.

11/ ON THE USEFULNESS OF COUPLED CHANNEL CALCULATIONS FOR ACTINIDE NUCLEI

Ch. Lagrange

Nuclear model calculations may be used to provide energy averaged neutron cross sections for actinide nuclei in case where no experimental data are available. The reliability of the calculated results obtained is related to our knowledge of the model and to the determination of the parameters.

The optical model is a basic calculational tool, and in the actinide mass region a physically coherent interpretation of the neutron interaction with deformed nuclei need deformed optical model (DOM) calculations. But the computer time involved in such calculations is often considered as prohibitively large. Because of this consideration spherical optical model (SOM) calculations have been carried out at various times [1,2,3]. As the model involves a relatively great number of parameters, it is indeed easy to obtain in selected energy ranges SOM calculations in good agreement with some restricted experimental data. But it turns out that the parameters thus obtained present one or two of the following anomalies : i/ different geometrical parameters at various energies [2], ii/ dependence of the real potential depth on the incident energy which is too small [3] (as for example .05E) or incoherent [1], (decreasing and then increasing), iii/ or a too small diffuseness of the real potential [1,3]. In optical model calculations a special attention is taken on the relation between the calculated compound nucleus (CN) formation cross section and the shape elastic cross section. For this purpose comparisons are made between calculated and measured quantities : elastic angular distributions at high enough energies and total cross sections.

It is worth while to mention that the "old experimental data" obtained by Batchelor et al [4] does not represent the "true" elastic angular distribution but the sum of elastic and inelastic from the first 2^+ and 4^+ states angular distributions. Thus crude comparisons of these data to SOM calculations would lead to an erroneous conclusion. We present in Fig. 1 the "true" elastic angular distribution calculated for ^{238}U at E_n = 3.40 MeV using SOM [1,3] and DOM [5] calculations together with experimental results from Haouat et al. [5]. The Fig. 2 shows at the same energy our DOM calculations of the elastic and inelastic scattering angular distributions. From the results presented in Fig. 2 it appears that a "SOM" fit to the "sum" of the scattering angular distributions would be meaningless as a representation of the expected elastic process. Let us assume that equivalent fits, using SOM and DOM parameters, were obtained to the "s" and "p"-wave strength functions and the neutron total cross sections over the full energy range 10 keV - 20 MeV. The CN cross section deduced is given by : $\sigma_{CN} = \sigma_{tot} - \sigma^{D}_{el}$ for the SOM calculations and : $\sigma_{CN} = \sigma_{tot} - \sigma^{D}_{el} - \sigma^{D}_{inel}$ for the "DOM" calculations. As the direct inelastic scattering cross sections (σ^{D}_{inel}) are greatly energy dependent : small at lower energies and not negligible at higher energies (for example 600 millibarns near 3.4 MeV), the deduction of C.N. (or elastic) cross sections from SOM fits to the total cross section is ambiguous and has no physical support. This is illustrated by the SOM (H. Matsunobu et al. [3], P. Lambropoulos [1]) and DOM calculations (Ch. Lagrange) of the C.N. formation cross sections for ^{238}U reported in Fig. 3. The differences in the various calculated results are greatly energy dependent, and a global renormalization of the SOM values to the DOM ones would be impossible and not suitable. Moreover, as noted by Konshin [6] in the case of ^{241}Pu, a renormalization on experimental data of the cross sections obtained from a statistical model calculation using transmission coefficients obtained from the SOM parameters of Lambropoulos, has been done at energies above 1 MeV. Such a renormalization appeared to be necessary, but the above considerations show how arbitrary can be the data to be chosen for it. And what could happen when experimental data are more scarce ?

One of the most important reasons for paying particular attention to the optical model parameterisation is the obtention of a parameter set suited for extrapolation to neighbouring nuclei. As noted by Matsunobu et al [3], the SOM calculations cannot reproduce the general trends of the s-and p-wave strength functions within the mass number region A = 232-241. These authors have obtained calculated values of these strength functions for ^{232}Th ($S_0 = 0.87$, $S_1 = 1.66$) in good agreement with the values given in Ref. [7] ($S_0 = 0.84 \pm 0.08$, $S_1 = 1.6 \pm 0.2$), but the values obtained for ^{239}Pu ($S_0 = 0.85$, $S_1 = 1.71$) are significantly smaller than the evaluated ones [7] ($S_0 = 1.3 \pm 0.1$, $S_1 = 2.3 \pm 0.4$). In these calculations only the depth of the real potential varies from nucleus to nucleus. Calculated values of compound nucleus formation cross section for ^{232}Th and ^{240}Pu using the SOM parameters of these authors and the DOM parameters from Ref. [5] and [8] are reported in Fig. 4. The inadequacy of SOM calculations for extrapolations within the actinide region is demonstrated by such examples.

Deformation effects on the neutron total cross sections are important and greatly energy dependent, and thus they could not be simulated by an unique and physically coherent SOM parameter set. Effects of quadrupole and hexadecapole deformation parameters on neutron total cross sections of actinide nuclei have been emphasized in Ref. [9] and [10] respectively. Some of the results obtained by these authors are presented in Fig. 5 and 6. From these examples it is demonstrated that for a precise evaluation of actinide neutron data, the existence of the quadrupole β_2 and hexadecapole β_4 should be taken into account. The effects of such deformation parameters on the calculation of the elastic and inelastic neutron scattering cross sections cannot be neglected either, as described in Chap. 4 of this report and Ref. [11] therein included. For DOM calculations the main changes of parameters from nucleus to nucleus concern only the deformation parameters. It is well known that significant comparisons have to be made using the multipole moments of the DOM instead of β_2 and β_4 directly. In this context microscopic calculations of deformation properties in the actinide region such as those recently performed by Girod and Gogny [12] are useful. Nevertheless, it is worth while to note that more theoretical calculations are needed concerning the deformation parameters of odd-A nuclei.

From the results presented above it is clear that SOM calculations are not to be recommended as a convenient tool for evaluating neutron cross sections in this mass region. In our opinion, when no coupled channel codes are available, interpolation or extrapolation of DOM published results, including generalized transmission coefficients needed for statistical model evaluation, seem to be more reliable than crude SOM calculations and have to be greatly recommended. We present in tables 1 and 2 examples of such an interpolation we have made. First DOM calculations for ^{234}U, ^{238}U and ^{242}Pu were made [13] and [8], and then the calculated results for ^{234}U and ^{242}Pu were averaged so as to obtain an "evaluation" for ^{238}U. Though the interpolation is crude the results presented in tables 1 and 2, where "averaged" and calculated results for ^{238}U can be compared, are unexpectedly satisfying. In order to facilitate such interpolations within the whole actinide region, we plan to make available [13] in the very near future our calculated DOM results for ^{234}U, ^{232}Th, ^{238}U and ^{248}Cm. We recall that our results for ^{240}Pu and ^{242}Pu have already been published [8]. We hope that such an effort will be fruitful in the framework of forthcoming actinide evaluations.

References of chapter 11

[1] P. Lambropoulos ; Nucl. Sci. Eng. 46 (1971) 356.

[2] S.B. Garg et al. ; Contribution at the Knoxville Conference (1979).

[3] H. Matsunobu et al. ; Contribution at the Knoxville Conference (1979).

[4] R. Batchelor et al. ; Nucl. Phys. 65 (1965) 236.

[5] G. Haouat et al. ; report NEANDC (E) 196 "L", INDC (FR) 29/L (1978).

[6] K.A. Konshin et al. ; report INDC (CCP) 142/GJ (1980)

[7] BNL-325, third edition, Vol. I, INDC (USA) - 58/L (1973).

[8] Ch. Lagrange, J. Jary ; report INDC (FR) 30/L (1978).

[9] Ch. Lagrange ; J. Phys. Letters 35 (1974) 111.

[10] K. Harada, and S. Igarasi ; in report AERE-R-8636 (1977).

[11] G. Haouat et al. ; in this report (chapter 4).

[12] M. Girod, and D. Gogny ; in this report (chapter 12).

[13] Ch. Lagrange ; to be published as an INDC report

	10 keV		0.5 MeV		1.0 MeV	
	averaged	calculated	averaged	calculated	averaged	calculated
σ_{tot}	15.822	15.803	8.549	8.539	6.973	6.963
$\sigma_{s.e}$	10.816	10.836	5.113	5.115	3.472	3.4828
σ_{NC}	5.006	4.967	3.320	3.310	3.225	3.2207
σ_{2+} (x 10^{+3})			106.97	104.95	208.86	203.19
σ_{4+} (x 10^{+3})			9.200	8.75	58.08	56.12

Comparisons of calculated and averaged neutron cross sections for ^{238}U (barn)

TABLE 1

ℓ,j	E_n = 0.01 MeV		E_n = 0.5 MeV		E_n = 1.0 MeV	
	averaged	calculated	averaged	calculated	averaged	calculated
0 1/2	0.6357 10^{-1}	0.63113 10^{-1}	0.3649	0.35784	0.46786	0.45868
1 1/2	0.3207 10^{-2}	0.31782 10^{-2}	0.4662	0.466122	0.6852	0.69295
1 3/2	0.43783 10^{-2}	0.43274 10^{-2}	0.5698	0.57639	0.7589	0.77255
2 3/2			0.9649 10^{-1}	0.94650 10^{-1}	0.24987	0.24452
2 5/2			0.8047 10^{-1}	0.77281 10^{-1}	0.2366	0.22861
3 5/2			0.1293 10^{-1}	0.12821 10^{-1}	0.1210	0.12145
3 7/2			0.1528 10^{-1}	0.1541 10^{-1}	0.1421	0.14302
4 7/2			0.2557 10^{-3}	0.28620 10^{-3}	0.5332 10^{-2}	0.51222 10^{-2}
4 9/2					0.5787 10^{-3}	0.56230 10^{-3}

Comparisons of calculated and averaged transmission coefficients for ^{238}U

TABLE 2

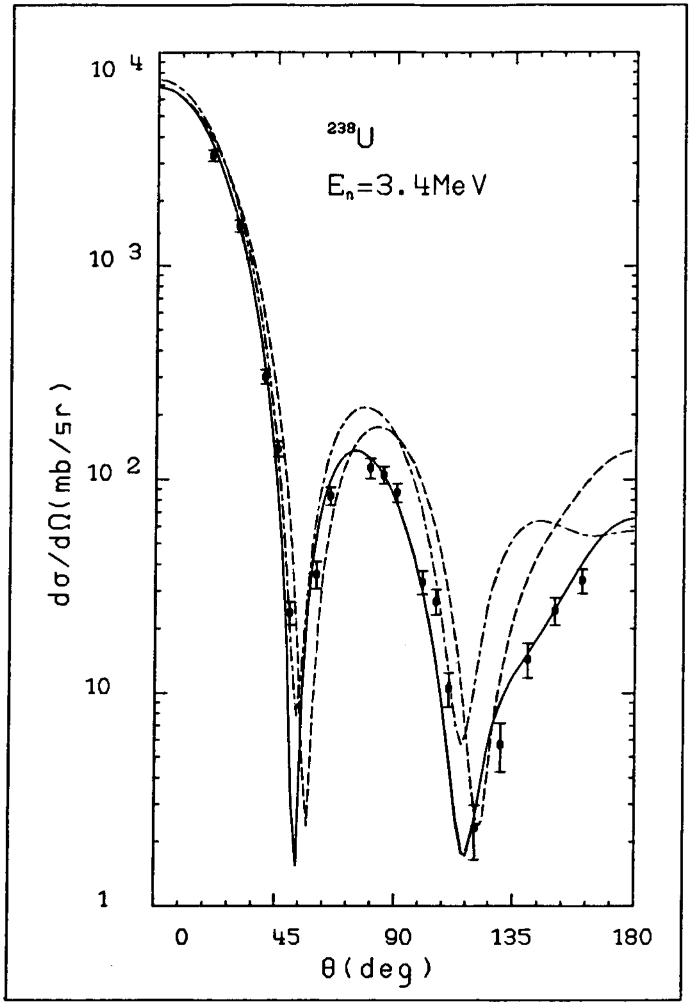

Fig. 1 - Differential scattering cross sections for ^{238}U (E_n = 3.4 MeV). Experimental data are from Ref. 5, calculated ones from Ref. 5 (full line), Ref. 1 (dashed line) and Ref. 3 (short dashed line).

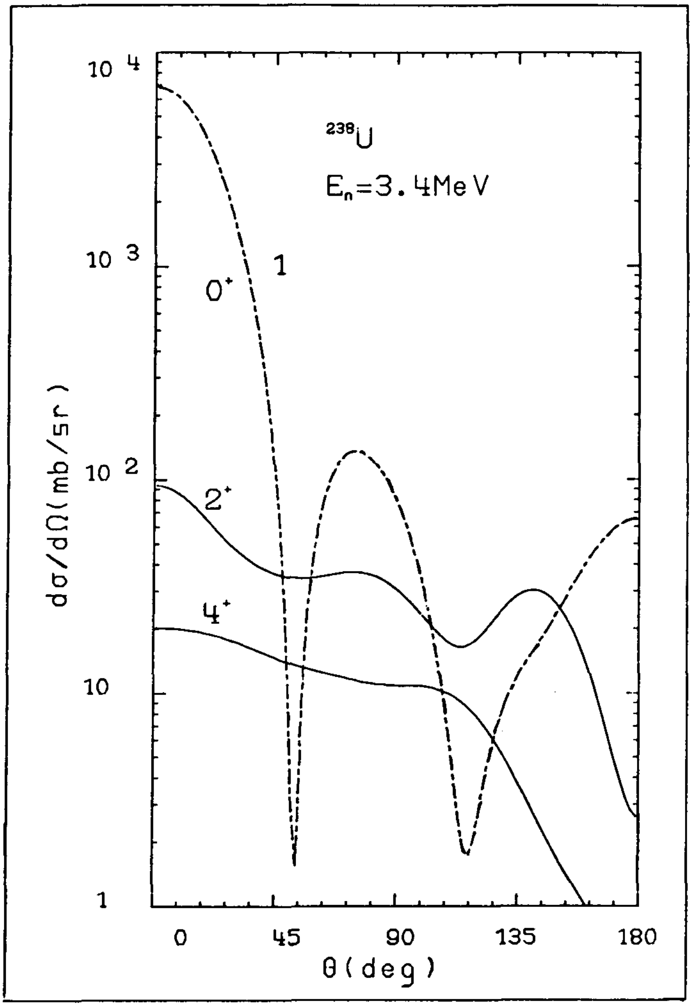

Fig. 2 - Neutron elastic and inelastic scattering calculated cross sections.

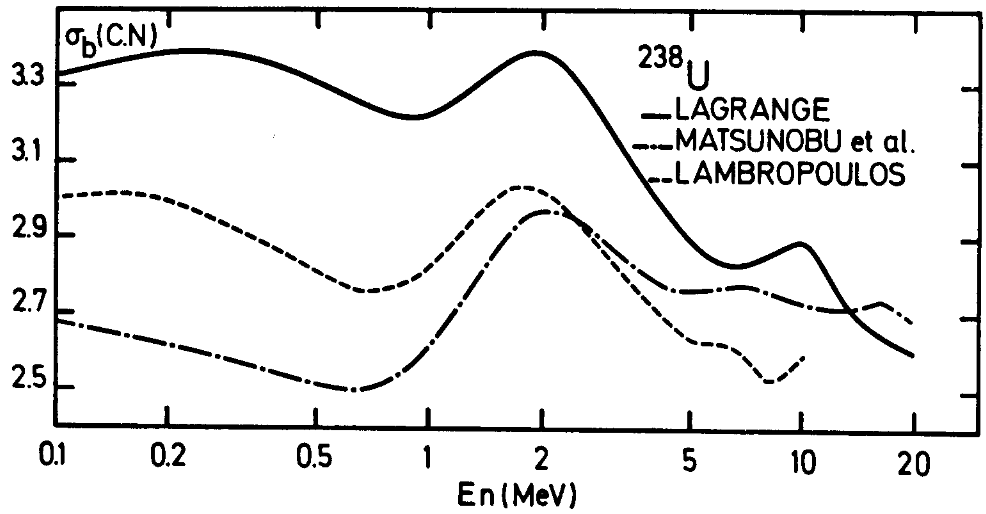

Fig.3 - Comparison of "SOM" and "DOM" calculated compound nucleus formation cross sections for ^{238}U.

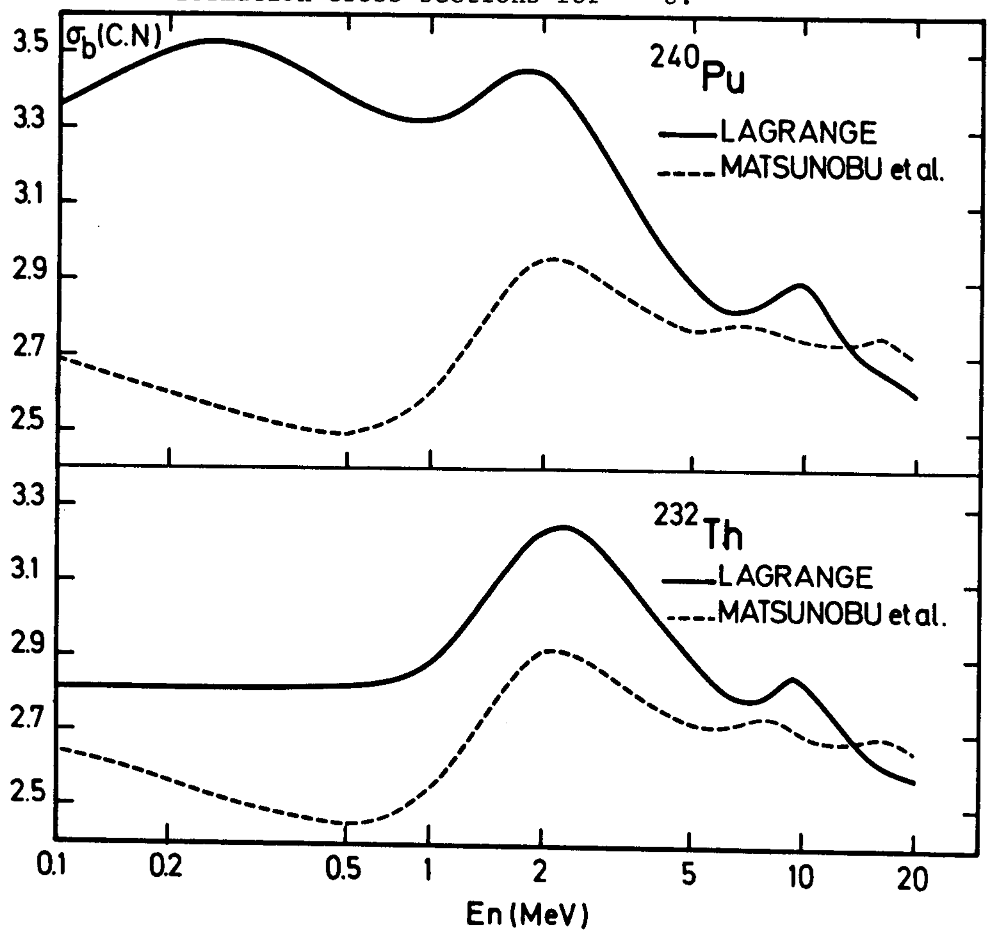

Fig. 4 - Comparison of "SOM" and "DOM" calculated compound nucleus formation cross sections for ^{240}Pu and 232Th.

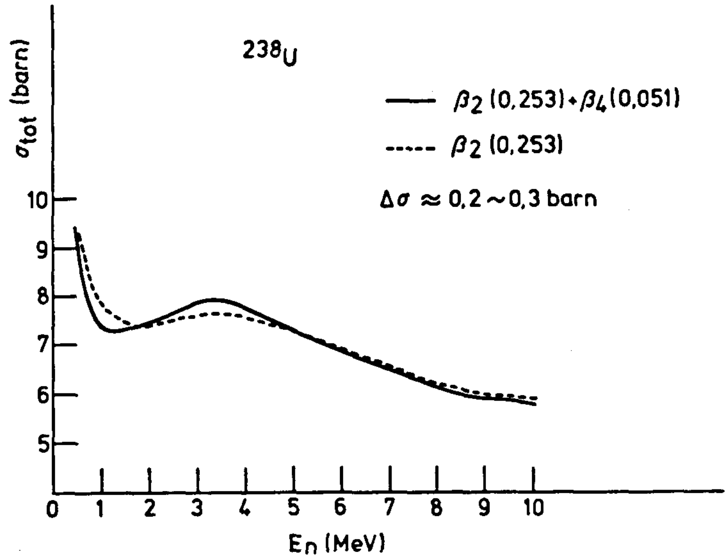

Fig. 5

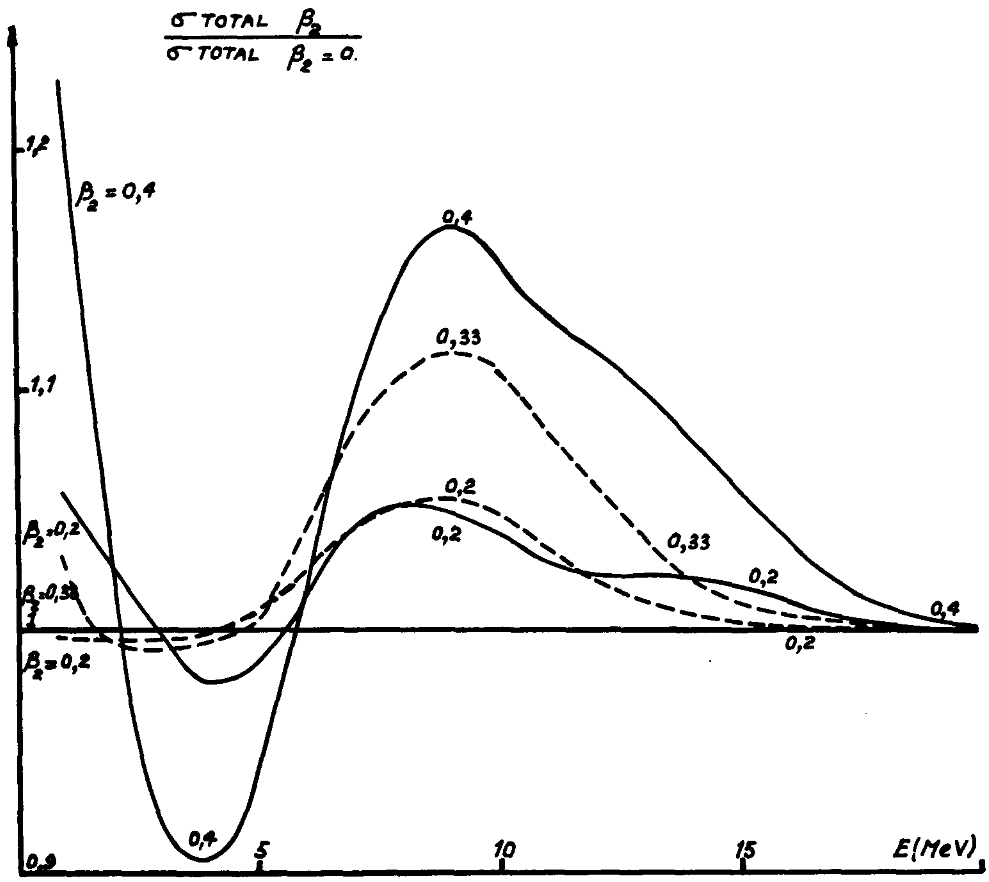

Fig. 6

Fig. 6 - Effect of the quadrupole deformation (β_2) on the neutron total cross section (cf. ref 9).

Fig. 5 - Effect of the hexadecapole deformation (β_4) on the neutron total cross section (cf. ref. 10).

12/ MICROSCOPIC CALCULATION OF DEFORMATION PROPERTIES IN THE ACTINIDE REGION

M. Girod and D. Gogny

In the last decade, Hartree-Fock (HF) type calculations with density dependent effective interactions have been performed in the whole chart of nuclides. The calculations, first undertaken for spherical nuclei, have been extended with a great success to the description of deformed ones.

Several interactions have been proposed up to now. The main bulk of the calculations have been performed with the Skyrme force SIII [1]. This zero-range force lends itself to fast calculations, but the counterpart of this simplicity is the impossibility to treat selfconsistently the pairing effects. Such effets are very important in the deformed nuclei on account of the high level-density near the Fermi level.

The calculations, presented here, have been performed with Gogny's D1 density dependent force [2]. This finite range interaction has been fitted in such a way as to permit the correct simultaneous treatment of the mean field and the pairing field in the framework of the Hartree-Fock-Bogolyubov approximation (HFB). The D1 interaction makes possible the description of a lot of spherical-nuclei properties (binding energy, charge radius, charge densities...) in the HF, HFB and HF + RPA approximations. We have also calculated many deformed nuclei from ^{8}Be to ^{248}Cm with this interaction [3].

We give here the preliminary results of HFB calculations for ^{232}Th, ^{240}Pu and ^{248}Cm.

The techniques of HFB calculations with a finite range interaction are evidently more complicated than HF calculations with zero-range force, where one avoids the time-consuming building up of matrix elements of the two body hamiltonian. But due to the separation method we developed in Ref. [4], we were, in fact, able to construct a very fast algorithm for the calculation of the matrix elements.

The HFB solutions are expanded in a deformed oscillator basis. The conserved symmetries are the axial symmetry and the left-right one. This basis is troncated with the usual prescription :

$$(2n_\perp + m + 1)\,\hbar\omega_\perp + (n_z + 1/2)\hbar\omega_z \leqslant (N + 2)\hbar\omega_0$$

where $\hbar\omega_0^3 = \hbar\omega_\perp^2 \cdot \hbar\omega_z$.

The parameters of the basis are $\hbar\omega_o$ and $q = \hbar\omega_\perp / \hbar\omega_z$. We must choose these parameters in order to minimize the HFB energy. It is clear, however, that for a sufficiently large number of shells N, the solutions are practically independant of these parameters.

The deformation properties are given in Table I for ^{232}Th, ^{240}Pu and ^{248}Cm. These results have been obtained by a self-consistent HFB calculation without any constraints (except for those imposed by the symmetries).

The convergence of the iterative method is fast for the binding energy but rather slow for the multipole moments. We stop the iteration procedure when the q_{40} variation is less than 10 fm^4.

We define the multipole moments by $q_{\lambda_o} = \langle HFB | r^\lambda Y_{\lambda o} | HFB \rangle$. They are connected to the usual β_λ parameters which enter the description of the nucleus surface through $R = R_o(1 + \beta_2 Y_{20} + \beta_4 Y_{40} + \beta_6 Y_{60})$ by the relation :

$$q_{\lambda_o} = \frac{3A}{4\pi R_o^3} \iint_o^R r^\lambda \, Y_{\lambda_o} \, r^2 dr d\Omega \qquad (R_o^2 = \frac{5}{3} \langle r^2_{HFB} \rangle)$$

This parameterisation, which assumes a sharp-edged surface, is a crude simulation of the nuclear density. The β_λ are somewhat model dependent, but their advantage lies in their simplicity.

The first column of the Table I gives the HFB binding energies calculated with a large oscillator basis (13 major shells). The differences with the experimental binding energies are no more than 4 MeV.

The second column gives the HFB neutron gap which is to be compared to the experimental gap : $2\Delta_n^{exp} = 2B(A) - B(A+1) - B(A-1)$ where B(A) is the experimental binding energy. Here also the comparison is satisfactory.

The next columns of the Table I display the ground state HFB results for the charge radius, the multipole moments $q_{\lambda_o} = \langle r_\lambda \, Y_{\lambda_o} \rangle$ and the deformation parameters β_λ . Various experimental and theoretical results are also presented for comparison.

The q_{20} moments are rather well reproduced but there are some disagreement concerning the hexadecapole moment of ^{248}Cm compared to Coulomb excitation data. The HFB deformations are very close to the deformations obtained with other theoretical calculations. (This is generally what happens for well deformed nuclei).

We are now calculating other nuclei in the actinide region. The corresponding results will be reported in a forthcoming publication.

References of chapter 12

[1] M. Beiner, H. Flocard, Nguyen Van Giai, P. Quentin ; Nucl. Phys. A238 (1975) 29.
P. Quentin and H. Flocard ; Ann. Rev. Part. Sci. (1978) 28, 523.

[2] D. Gogny (1975) ; Nuclear Self Consistent Fields, ed. G. Ripka, M. Porneuf p. 333, Amsterdam, North Holland.
J. Dechargé and D. Gogny ; Phys. Rev. C21 (1980) p. 1568.

[3] J. Dechargé, M. Girod, D. Gogny ; Phys. Lett. B55 (1975) 361.
M. Girod and D. Gogny ; Phys. Lett. B64 (1976) 5, and to be published.

[4] D. Gogny ; Nucl. Phys. A237 (1975) 399.

TABLE I

	B (MeV)	Δ_n (MeV)	r_{ch} (fm)	q^P_{20} (b)	q^M_{20}	q^P_{40} (b^2)	q^M_{40}	q^P_{60} (b^3)	q^M_{60}	$<r^2_{HFB}>^{1/2}$ (fm)	β^P_2	β^M_2	β^P_4	β^M_4	β^P_6	β^M_6
^{232}Th	1765.7	.93	5.761	2.79	7.32	.87	2.3	.19	.48	5.767	.201	.204	.084	.085	.016	.014
	1766.709[a]	.83[a]	5.773[b]		8.164[c]		3.161[c]		.804[c]		.216[d]		.111[d]			
				3.04[e]		1.22±.15[e]					.206[f]		.084[f]			
				3.05[h]												
				3.04±.14[i]		1.21±.12[i]										
^{240}Pu	1811.7	.90	5.850	3.47	8.76	1.02	2.54	.18	.38	5.849	.230	.228	.078	.077	.002	−.003
	1813.475[a]	.65[a]		3.65[e]		1.15±.28[e]					.250[d]		.082±.029[d]			
				3.56[h]							.229[f]		.064[f]			
				3.33±.15[i]		1.16±.11[i]					.241[g]	.239[g]	.079[g]	.078[g]		
^{248}Cm	1856.2	.80	5.914	3.74	9.60	.68	1.64	.01	−.06	5917	.245	.245	.030	.026	−.020	−.025
	1859.215[a]	.75[a]		3.87[e]		$0.^{+.5}_{-.6}$[e]					.284[d]		−.044±.059[d]			
											.246[f]		.032[f]			
											.257[g]	.259[g]	.028[g]	.022[g]		

- The top entries for each nucleus denote HFB predictions -

(a) *Atomic data and Nuclear Data Tables* 19, 177 (1977).
(b) " " " 14, 479 (1974).
(c) F.A. Brieva and B.Z. Georgiev; Nucl. Phys. A308, 27 (1978).
(d) W.T. Milner, C.E. Benis and F.K. Gowan; Phys. Rev. C16, 1686 (1977).
(e) C.E. Bemis et al.; Phys. Rev. C8, 1466 (1973).
(f) S.G. Nilsson et al.; Quoted in (e).
(g) P. Quentin and H. Flocard, Ann. Rev. Part. Sci. 28, 523 (1978).
(h) K.E.G. Löbner, M.Vetter and V. Hönig; Nuclear Data A7, 5 (1970).
(i) Ch. Lagrange; private communication.